ACS APPLIED ENERGY MATERIALS

www.acsaem.org Article

Poly(ether sulfone)-Based Anion Exchange Membranes Containing Dense Quaternary Ammonium Cations and Their Application for Fuel Cells

Ping-Yen Chen, Tse-Han Chiu, Jyh-Chien Chen,* Kai-Pin Chang, Shih-Huang Tung, Wei-Tsung Chuang, and Kuei-Hsien Chen

Cite This: *ACS Appl. Energy Mater.* 2021, 4, 2201−2217 Read Online

ACCESS | Metrics & More | Article Recommendations | Supporting Information

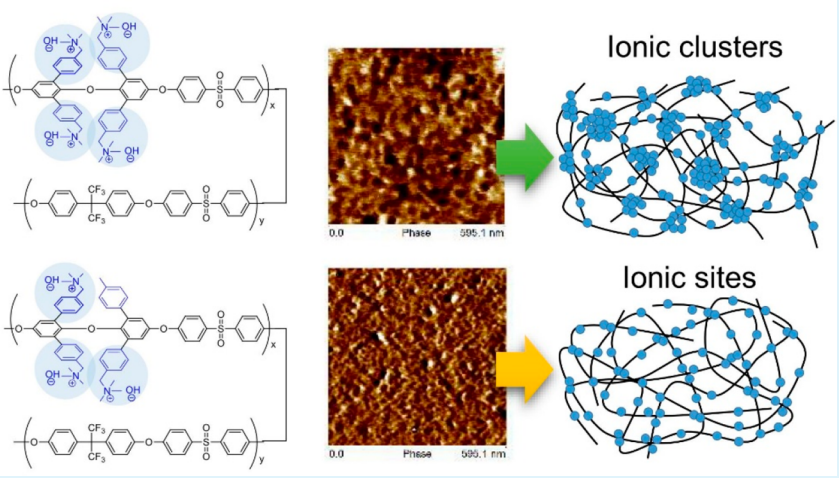

ABSTRACT: Poly(ether sulfone)-based anion exchange membranes (AEM)s containing dense quaternary ammonium cations were prepared for anion exchange membrane fuel cell applications. Poly(ether sulfone)s, XMePh-Z, derived from a new aromatic diol, 4,4′-dihydroxy-2,2′,6,6′-tetra(*p*-tolyl)diphenyl ether containing four tolyl substituents, 4,4′-(hexafluoroisopropylidene)diphenol (HFDP), and bis(4-fluorophenyl)sulfone (BFS), were prepared and functionalized via photoinitiated bromination on tolyl substituents followed by quaternization. The photoinitiated bromination is so selective that the reaction occurred only on the methyl groups of tolyl substituents without polymer main chain degradation. The IEC values of poly(ether sulfone)-based AEMs, from 1.21 to 2.11 mmol/g, can be controlled by the degree of bromination. These membranes with water uptake from 40 to 120% exhibited hydroxide conductivity at 80 °C from 13 to 45 mS/cm. By using different ratios of monomers with and without tolyl substituents, the distribution of cationic groups can be controlled. AEMs with a smaller amount of tolyl-substituted monomer had their cationic sites located more closely when IEC values were the same. This allowed membranes with the same IEC values exhibited lower water uptake, better dimensional stability, and higher hydroxide conductivity. These AEMs also demonstrated good alkaline stability. In the case of 40MePh-1.72 with an IEC value of 1.72 mmol/g, the hydroxide conductivity and IEC remained at 78 and 81% of their original values, respectively, after 720 h of an alkaline stability test. A single fuel cell based on 40MePh-1.72 exhibited an open circuit voltage of 1.03 V and peak power density of 291 mW/cm^2 at 60 °C using platinum loading of 0.5 mg/cm^2. It performed better than a single fuel cell based on commercially available FAA-3 with an open circuit voltage of 1.02 V and peak power density of 226 mW/cm^2 under the same testing conditions.

KEYWORDS: *anion exchange membrane, ion conductivity, fuel cell, ionic cluster, poly(ether sulfone)s*

1. INTRODUCTION

Polymer electrolytes, which were first introduced by Fenton and co-workers in 1973,[1] consist of polymeric materials as a matrix and ionic sites fixed to the matrix by covalent bond. Because of their applications in energy conversion/storage system,[2,3] water treatment, and hydrogen production,[4] polymer electrolytes have attracted intensive research efforts in last

Received: November 3, 2020
Accepted: February 24, 2021
Published: March 10, 2021

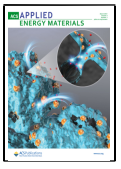

https://dx.doi.org/10.1021/acsaem.0c02734
ACS Appl. Energy Mater. 2021, 4, 2201−2217

several decades. Compared to conventional liquid electrolytes, polymer electrolytes have several advantages such as being solvent-free, lightweight, and flexible and having a membrane-forming ability, high ionic conductivity, and a wide electrochemical window. In addition, polymer electrolytes diminish the problems associated with liquid electrolytes such as electrolyte leakage, internal shorting, corrosion, production of harmful gases and the presence of nonflammable products.[5] In particular, polymer electrolytes are usually employed in H_2/O_2 polymer electrolyte membrane fuel cells, which exhibit high conversion efficiency, high energy density, low emission, and wide applications as portable, stationary, automotive power sources.

Among various fuel cells, proton exchange membrane fuel cells (PEMFCs) have drawn much attention because of their applications in transportation and portable electronics.[6] However, because of the high cost of the membranes and electrochemical catalysts and sparse coverage of the hydrogen supply, a large-scale adoption of PEMFCs has yet to be realized.[7,8] In recent years, researches on anion exchange membrane fuel cells (AEMFCs) have sprung up.[9,10] Anion exchange membranes (AEMs) are employed as electrolytes to transfer hydroxide ion and separate fuel gases in AEMFCs. It is more important that oxygen reduction reaction (ORR) kinetics is faster in alkaline condition. Thus, the potential use of nonprecious metals (e.g., silver, nickel, and cobalt) as electrochemical catalysts in AEMFCs might eventually realize the large-scale commercialization of fuel cells at inexpensive cost.[11]

However, new challenges emerge when anion exchange membranes are employed in fuel cells. Hydroxide ions in AEMs originate from the counterions of quaternary ammonium salts and the product of cathodic oxygen reduction. The dissociation of hydroxide ions from quaternary ammonium salts in AEMs is obviously poorer than that of protons from sulfonic acids in proton exchange membranes (PEMs). Besides, some articles reported that the transport of hydroxide ion is only about half the rate of proton in aqueous solution.[12,13] Improving hydroxide conductivity is pursued by various chemical structure designs and morphology controls in numerous researches.[14−18] Furthermore, excellent alkaline stability of AEMs becomes a rigorous qualification because the cationic sites and polymer main chains are possibly attacked by hydroxide ions.[11,19,20] To develop an AEM with both outstanding hydroxide conductivity and alkaline stability as polymer electrolyte used in AEMFCs remains a challenging task. To improve the hydroxide conductivity of AEMs, polymers consisting of both hydrophilic and hydrophobic segments by block copolymerization or structures containing highly localized cationic groups were prepared.[21−27] Jannasch and co-workers reported poly(ether sulfone)-based anion exchange membranes containing di-, tri-, tetra-, and hexa-cationic groups clustering in a repeat unit.[21,23,24,26] It was found that the quaternary ammonium groups located more densely at specific phenylene rings in the polymer backbones, the membranes absorbed less water. The hydroxide conductivity of copolymers was boosted by the formation of hydrophilic domains from dense ionic clusters in comparison to homopolymers that were functionalized randomly.

In this study, poly(ether sulfone)s, XMePh-Z, derived from a new aromatic diol, 4,4′-dihydroxy-2,2′,6,6′-tetra(*p*-tolyl)-diphenyl ether containing four tolyl substituents, 4,4′-(hexafluoroisopropylidene)diphenol (HFDP) and bis(4-fluorophenyl)sulfone (BFS) were prepared and functionalized via photoinitiated bromination on tolyl substituents followed by quaternization. By this specific bromination, only the methyl groups of tolyl substituents were brominated without polymer main chain degradation. This unique chemical structure allows us to prepare AEMs in different distributions of cationic groups with similar IEC values by adjusting the monomer molar ratio. The properties of AEMs, such as ion exchange capacity (IEC), water uptake (WU), dimensional change, hydroxide conductivity, morphology, alkaline stability, and fuel cell performance are investigated. The relationship between membrane properties, copolymer composition, and degree of functionalization is also studied. The good performance of a single anion exchange membrane fuel cell based on these membranes is also demonstrated.

2. EXPERIMENTAL SECTION

2.1. Materials. Monomer, 4,4′-dihydroxyl-2,2′,6,6′-tetraphenyldiphenyl ether **1**, was prepared according to our previous study.[28] Chloroform, dimethyl sulfoxide (DMSO), *N*,*N*-dimethylacetamide (DMAc), and *N*,*N*-dimethylformamide (DMF) were purchased from Tedia. *p*-Tolylboronic acid and (2,4,6-trimethyl benzoyl) diphenyl phosphine oxide was purchased from Sigma-Aldrich. *N*-Bromosuccinimide, bis(4-fluoro-phenyl)sulfone, paraformaldehyde, $Pd(PPh_3)_4$, and stannic chloride (anhydrous) were purchased from Acros. 40% Pt/C (Johnson Matthey, HiSPEC 4000), 10% Pd/C were purchased from Alfa Aesar. FAA-3 membrane and its ionomer solution (10% in NMP) were purchased from FuMATech. Carbon papers (GDL-39BC) were purchased from SGL Group. Other chemicals were obtained from common suppliers. All chemicals were used as received unless specified otherwise.

2.2. Synthesis of Monomer. *2.2.1. 4,4′-Dinitro-2,2′,6,6′-tetra(p-tolyl)diphenyl Ether* ***2.*** 2,2′,6,6′-Tetrabromo-4,4′-dinitrodiphenylether[29] (5.00 g, 8.68 mmol) and toluene (50 mL) were stirred in a 250 mL, three-necked, round-bottomed flask equipped with a nitrogen inlet, a thermometer, and a condenser at 80 °C until a homogeneous solution was obtained. The solution was vigorously stirred for 60 min after adding a sodium carbonate aqueous solution (7.70 g, in 32 mL of water) and $Pd(PPh_3)_4$ (1.20 g). A solution of *p*-tolylboronic acid (9.50 g, 69.87 mmol) in ethanol (40 mL) was added and the solution was vigorously stirred and heated at 110 °C for 48 h. The reaction mixture was then filtered through a short Celite pad to remove the insoluble components. The filtrate was washed several times with a saturated NaCl aqueous solution and dried with anhydrous magnesium sulfate. The Celite pad was washed by CH_2Cl_2 until the filtrate was colorless. After the combined filtrates were concentrated by rotary evaporator, the crude product was purified by a short column using dichloromethane as the eluent to afford a brown solid. The brown solid was washed by acetone and recrystallized in toluene to afford 3.77 g of yellow crystal (yield: 70%). Mp: 252−255 °C. ^{1}H NMR (600 MHz, $CDCl_3$, δ, ppm): 2.41 (s, 12H), 7.18 (d, J = 7.8 Hz, 8H), 7.22 (d, J = 7.8 Hz, 8H), 7.74 (s, 4H). ^{13}C NMR (150 MHz, DMSO-d_6, δ, ppm): 21.4, 125.5, 128.9, 133.4, 134.1, 138.5, 143.1, 154.7. EIMS (m/z): calcd for $C_{40}H_{32}N_2O_5$, 620.2; found, 620.2 $[M]^+$. Anal. Calcd for $C_{40}H_{32}N_2O_5$: C, 77.40; H, 5.20; N, 4.51; O, 12.89. Found: C, 77.10; H, 5.40; N, 4.54; O, 12.96.

2.2.2. 2,2′,6,6′-Tetra(p-tolyl)-4,4′-oxydianiline ***3.*** Compound **2** (3.00 g, 4.83 mmol), ethyl acetate (24 mL), ammonium formate (3.40 g, 53.92 mmol), ethanol (24 mL), and Pd/C (0.40 g, 10 wt %) were stirred in a 100 mL, three-necked, round-bottomed flask equipped a condenser at room temperature for 24 h. The reaction mixture was then filtered through a short Celite pad to remove the insoluble components. The filtrate was collected and washed several times with a saturated NaCl aqueous solution. The organic solution was dried with anhydrous magnesium sulfate, concentrated by rotary evaporator, and dried under reduced pressure at 120 °C for 12 h to afford 2.63 g of solid (yield: 97%). Mp: 231−234 °C. ^{1}H NMR (600 MHz, DMSO-d_6, δ, ppm): 2.34 (s, 12H), 4.50 (s, 4H), 6.00 (s, 4H), 7.04 (d,

https://dx.doi.org/10.1021/acsaem.0c02734
ACS Appl. Energy Mater. 2021, 4, 2201−2217

J = 8.0 Hz, 8H), 7.16 (d, J = 8.0 Hz, 8H). ^{13}C NMR (150 MHz, DMSO-d_6, δ, ppm): 20.8, 115.6, 127.7, 128.9, 132.0, 136.3, 141.7, 142.7. EIMS (m/z): calcd for $C_{40}H_{36}N_2O$, 560.3; found, 560.3 $[M]^+$. Anal. Calcd for $C_{40}H_{36}N_2O$: C, 85.68; H, 6.47; N, 5.00; O, 2.85. Found: C, 85.16; H, 7.30; N, 4.62; O, 2.92.

2.2.3. 4,4′-Dihydroxy-2,2′,6,6′-tetra(p-tolyl)diphenyl Ether 4. A 50% sulfuric acid solution (30 mL) and compound **3** (3.00 g, 5.34 mmol) were stirred in a flask under a N_2 atmosphere at room temperature until a homogeneous solution was obtained. A sodium nitrite ($NaNO_2$) aqueous solution (0.90 g in 1 mL of deionized water) was added and the solution was cooled in an ice bath for 30 min. The solution was then added slowly by droplet into a presettled 50% sulfuric acid solution, which was heated at 160 °C in advance. After the reaction mixture was heated at 160 °C for 10 min, it was poured into ice. The aqueous solution was extracted by ethyl ether. The organic solution was washed with water, dried with anhydrous magnesium sulfate, and concentrated by rotary evaporator. The crude product was purified by column chromatography using hexane/THF (5/2, v/v) as the eluent and then recrystallized in $CHCl_3$/hexane (1/1, v/v) to afford 0.60 g of colorless crystal (yield: 27%). Mp: 219−220 °C. ^{1}H NMR (600 MHz, DMSO-d_6, δ, ppm): 2.34 (s, 12H), 6.16 (s, 4H), 7.05 (d, J = 8.0 Hz, 8H), 7.19 (d, J = 8.0 Hz, 8H), 8.85 (s, 2H). ^{13}C NMR (150 MHz, DMSO-d_6, δ, ppm): 20.8, 116.2, 127.9, 128.8, 132.5, 135.6, 135.7, 143.0, 151.5. EIMS (m/z): calcd for $C_{40}H_{34}O_3$, 562.3; found, 562.2 $[M]^+$. Anal. Calcd for $C_{40}H_{34}O_3$: C, 85.38; H, 6.09; O, 8.53. Found: C, 85.07; H, 6.32; O, 8.61.

2.3. Synthesis of Poly(ether sulfone)s XPh and XMePh. Poly(ether sulfone)s (PES) were synthesized via aromatic nucleophilic substitution from monomer **1** (ormonomer **4**), 4,4′-(hexafluoroisopropylidene)diphenol (HFDP), and bis(4-fluorophenyl)sulfone (BFS). Copolymers with various compositions were prepared based on different molar ratios of monomer **1** (ormonomer **4**) to HFDP. The copolymers are designated as XPh and XMePh, where X represents the percentage of the repeating units derived from monomer **1** and **4** in copolymers, respectively. The synthesis of 60MePh as an example is described in the following procedures. Monomer **4** (0.8746 g, 1.55 mmol), HFDP (0.3484 g, 1.04 mmol), BFS (0.6586 g, 2.59 mmol), K_2CO_3 (0.7876 g, 5.70 mmol), DMAc (9.4 mL), and toluene (4.7 mL) were mechanically stirred in a three-necked flask equipped with a Dean−Stark apparatus, a condenser, and a N_2 inlet at 130 °C for 4 h. The reaction mixture was then heated at 160 °C for 24 h. The water that formed was removed by azeotropic distillation. The viscous solution was then poured into water. The fibrous polymer was collected and washed with hot water and hot ethanol. The fibrous polymer was then dried at 100 °C under reduced pressure overnight (yield: 96%).

XPh and XMePh were then chloromethylated (on phenyl group) and brominated (on methyl group), respectively, to form methylene halide. The degree of chloromethylation and bromination is defined as the number of chloromethyl and bromomethyl group in the repeating unit derived from monomers **1** and **4**, respectively. The functionalized XPh and XMePh are named as XPh-YCl and XMePh-YBr, respectively, where Y is the average number of chloromethyl and bromomethyl groups in the repeating unit derived from monomers **1** and **4**, respectively. Y was determined from the corresponding ^{1}H NMR spectrum. For instance, functionalized 60MePh with 3.40 bromomethyl groups per repeating unit derived from monomer **4** is expressed as 60MePh-3.40Br.

2.4. Functionalization of PESs. *2.4.1. Chloromethylation of XPh.* Chloromethylated poly(ether sulfone) was synthesized by a Friedel−Crafts like reaction referred to a previous article.[30] The typical procedures of XPh-YCl are described in the following. Paraformaldehyde, chlorotrimethylsilane, and then anhydrous stannic chloride were added into chloroform in a 100 mL flask with a magnetic stirrer. The reaction mixture was stirred at 60 °C to allow paraformaldehyde to completely dissolve, then was cooled to room temperature. XPh was added and the mixture was further stirred at 60 °C for 24 h. The feed ratio of reaction ingredients varied to control the degree of chloromethylation and in an attempt to avoid main chain scission. The reaction mixture was then poured into rigorously stirred methanol. The product was collected by filtration and dried under reduced pressure at 50 °C for 12 h (yield: 73−81%).

2.4.2. Bromination of XMePh. Poly(ether sulfone)s XMePh with various degrees of bromination were prepared by using a photoinitiator, (2,4,6-trimethylbenzoyl)diphenylphosphine oxide (TPO), with different amounts of *N*-bromosuccinimide (NBS) in 1,1,2,2-tetrachloroethane (TCE) under 254 nm UV light radiation without heating. The synthetic procedures of 60MePh-3.40Br are described as the example. 60MePh (0.60 g, 2.10 mmol methyl groups), TPO (0.024 g, 0.069 mmol), NBS (0.48 g, 2.69 mmol), and TCE (24 mL) were stirred in a100 mL, three-necked flask equipped with a nitrogen inlet and outlet, a condenser, and a mechanical stirrer for 24 h. The reaction mixture was exposed to UV light (254 nm) during stirring and then poured into methanol. The precipitate was collected, washed with methanol, and dried at 50 °C under reduced pressure overnight (yield: 92−96%).

2.4.3. Quaternization of Brominated Poly(ether sulfone) (XMePh-Z). A brominated poly(ether sulfone)s (XMePh-YBr) was dissolved in DMF at a concentration of 5% (w/v) followed by adding 5 equiv (relative to bromide) of trimethylamine (30% trimethylamine aqueous solution). The solution was stirred for 48 h and then poured into acetone. The precipitate was collected, washed with acetone and dried at 80 °C under reduced pressure overnight (yield: 97%). The quaternized polymers are named as XMePh-Z, where Z is the corresponding IEC value that was determined from the result of titration.

2.5. Membrane Fabrication and Anion Exchange. Quaternized poly(ether sulfone)s were dissolved in DMF with a solid content of 5% (w/v). The polymer solutions were filtered by a filter (0.45 μm) and then cast on a clean Petri dish. The solvent was evaporated at 50 °C on a hot plate under nitrogen atmosphere. The membranes were peeled off and soaked in distilled water for 2 h and further dried at 100 °C under reduced pressure for 6 h. The thickness of membranes was controlled in the range of 50−60 μm.

After being cut into specific sizes for different measurement, the membranes were immersed into a N_2-exposed NaOH aqueous solution (1.0 M) at room temperature for 3 days to exchange the anions from bromide to hydroxide. In this period of time, NaOH solution was refreshed every 12 h. The membranes were then washed with N_2-exposed deionized water and stored in N_2-exposed deionized water before used.

2.6. Measurements of Membrane Properties. *2.6.1. Ion Exchange Capacity (IEC) Measurement.* IEC_{NMR} and $IEC_{titr.}$ values were determined by ^{1}H NMR spectra and back-titration method, respectively. The procedures of $IEC_{titr.}$ measurement are described as following. AEM membrane (30−40 mg) was soaked in a deionized and N_2-exposed water, which was added calculated amount of $HCl_{(aq)}$ (the amount of HCl was 5 equiv relative to one equiv of quaternary ammonium groups calculated from IEC_{NMR}), for 48 h. The HCl solution was than titrated with a standardized 0.03 M NaOH solution on a titration meter (Metrohm 888 titrando). The $IEC_{titr.}$ value was calculated by eq 1:

$$IEC_{titr.}(\text{mmol/g}) = ({N_{HCl}}^0 - M_{NaOH}V_{NaOH})/W_{dry} \quad (1)$$

where ${N_{HCl}}^0$, M_{NaOH}, and V_{NaOH} are moles of HCl added initially, the molarity, and the volume of consumed NaOH solution, respectively. W_{dry} is the weight of dry membrane.

2.6.2. Water Uptake (WU) and Dimensional Change. The water uptake of the membranes was defined as the percentage of the weight change (ΔW) after anion exchange to the initial dry weight (W_{dry}) as given by eq 2:

$$WU(\%) = \Delta W/W_{dry}100\% \quad (2)$$

The dimensional change of the membrane after adsorbing water was measured by length change (LC) and thickness change (TC) in percentage. They are defined by eqs 3 and 4:

$$LC(\%) = \Delta L/L100\% \quad (3)$$

$$TC(\%) = \Delta T/T100\% \quad (4)$$

https://dx.doi.org/10.1021/acsaem.0c02734
ACS Appl. Energy Mater. 2021, 4, 2201−2217

Scheme 1. Synthetic Route of 4,4′-Dihydroxy-2,2′,6,6′-tetra(*p*-tolyl)diphenyl Ether 4

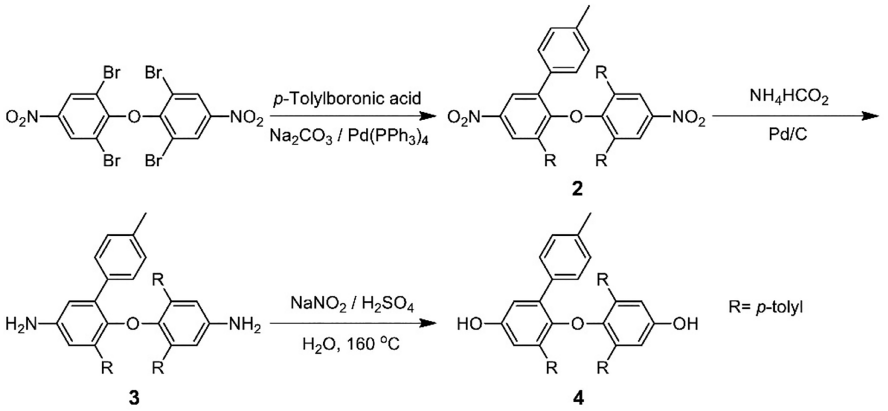

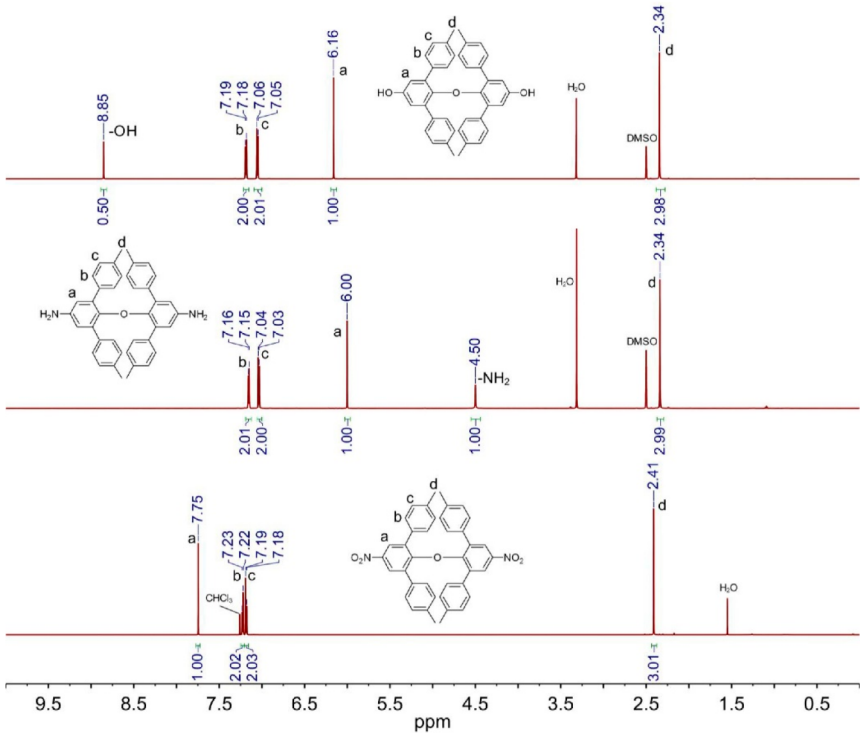

Figure 1. ^{1}H NMR spectra of compound **2** (bottom, $CDCl_3$), **3** (middle, DMSO-d_6), and **4** (top, DMSO-d_6).

where ΔL, L, ΔT, and T are length change, initial length, thickness change, and initial thickness, respectively.

2.6.3. Hydroxide Conductivity. The impedance of membranes in hydroxide form was measured using a two-electrode in-plane method by electrochemical impedance spectroscopy (EIS) with a Zahner potentiostat−galvanostat electrochemical workstation model PGSTAT over a frequency range of 1 Hz to 100 kHz with an oscillating voltage of 10 mV. A rectangle membrane (1 cm × 2 cm) was fixed in a homemade Teflon cell with two gold electrodes. The cell was set in an oven with a temperature and humidity controller. Each impedance was recorded at a specific temperature and relative humidity after the membrane stayed at that environment for 1 h. Hydroxide conductivity (σ) was calculated from the impedance data according to eq 5:

$$\sigma = d/(Rtw) \tag{5}$$

where σ is the hydroxide conductivity (S cm^{-1}), d is the distance between the electrodes, and t and w are the thickness (cm) and width (cm) of the sample, respectively. R is the resistance (Ω) associated with the ionic conductivity of the sample from the impedance data.

2.6.4. Alkaline Stability Test. The alkaline stability of membranes was evaluated by immersing membranes in N_2-exposed NaOH aqueous solution (1.0 M) at 60 °C. After a certain period of alkaline treatment, the membranes were taken out and washed with N_2-exposed deionized water until neutralization. The conductivity (at 80 °C and 98%RH) and $IEC_{titr.}$ of the membranes were measured. The membranes were then immersed in the N_2-exposed NaOH aqueous solution (1.0 M) at 60 °C again for subsequent tests.

2.6.5. Fabrication of Membrane Electrode Assembly and Fuel Cell Test. A polymer solution (5%, w/v) in DMF (180 μL) was dropped in a mixture of IPA (3 mL) and acetonitrile (2.7 mL). Catalyst inks were prepared by mixing the solution and catalyst under ultrasonic vibration for 2 h. The weight ratio between catalyst (Pt/C) and polymer was controlled at 4:1. The catalyst inks were then deposited on membranes by micropipette. During the deposition of catalyst ink, the solvents were removed by hot-air flow simultaneously. The catalyst-coated membranes (CCMs) were then dried at 100 °C under reduced pressure. The catalyst loading was calculated according to the weight change of membranes before and after catalyst deposition. In the case of FAA-3 membrane, the ionomer solution was

https://dx.doi.org/10.1021/acsaem.0c02734
ACS Appl. Energy Mater. 2021, 4, 2201−2217

Scheme 2. Synthetic Route of Polyethersulfones, XPh and XMePh

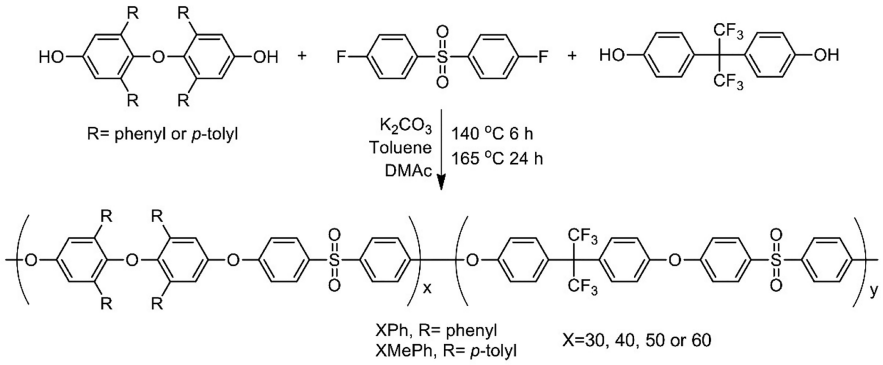

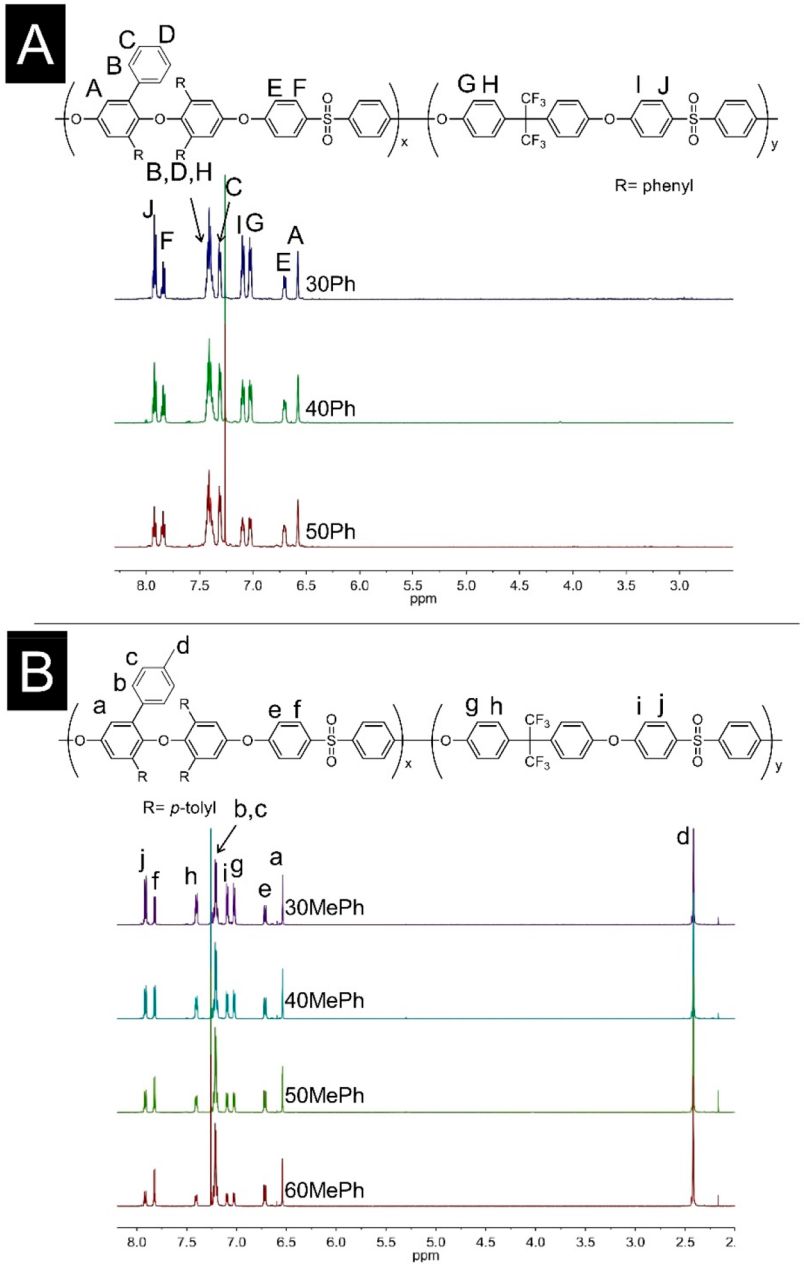

Figure 2. [1]H NMR spectra of poly(ether sulfone)s, (A) XPh and (B) XMePh.

composed of 10 wt % FAA-3 solution in NMP (0.09 g) and IPA (5.7 mL). The corresponding catalyst ink and CCM were prepared by the same way. CCMs were immersed in 1 M NaOH for 48 h, washed with deionized water to neutral, and then stored in deionized water. The

https://dx.doi.org/10.1021/acsaem.0c02734
ACS Appl. Energy Mater. 2021, 4, 2201−2217

CCMs were sandwiched between two carbon papers (SGL, GDL-39BC) without hot press. The active area of MEAs was 1 cm^2. H_2 (87%RH) and O_2 (91%RH) were introduced into the anode and cathode, respectively, with a flow rate of 0.2 L/min. No back pressure was applied.

2.7. Measurement. Melting points of monomers were measured on a Mel-Temp capillary melting point apparatus. Proton (^{1}H NMR) and carbon (^{13}C NMR) nuclear magnetic resonance spectra were analyzed on a Bruker Avance-600 spectrometer at 600 and 150 MHz, respectively. Mass analysis of monomers was conducted on a high-resolution mass spectrometer (JEOL JMS-700). Elemental analyses were completed on a Heraeus Vario analyzer. Molecular weights of polymers were measured on a JASCO GPC system (PU-980) equipped with an RI detector (RI-930), a Shodex GPC KF-804 column, using dimethylacetamide (DMAc) as the eluent and calibrated with polystyrene standards. Thermal gravimetric analyses (TGA) were performed under nitrogen flow in a TA TGA Q500 thermogravimetric analyzer using a heating rate of 10 °C min^{-1}. Mechanical properties of membranes were determined by a Universal Testing Machine (Testometric M500−25AT) at a cross-head speed of 5 mm min^{-1} under an atmosphere of 30−40% RH at 25 °C. The initial shape of membranes for mechanical properties measurement was rectangle (40 mm in length, 10 mm in width, and 30−50 μm in thickness). Morphology of the membrane surface was detected by AFM tapping-mode with a Bruker Dimension ICON in air, using a commercial Si cantilevers with a force constant of 7.4 N/m and resonance frequency of 160 kHz (Nanosensors, PPP-NCSTR). All of images containing 512 scan lines were performed at scan rate of 1.00 Hz and the height difference of them was below 3 nm, which would not affect the quality of phase images. Small-angle X-ray scattering (SAXS) was conducted at the beamline BL23A1 (National Synchrotron Radiation Research Center (NSRRC), Taiwan) using an X-ray source with a wavelength of 0.124 nm. The scattering intensity profiles were reported as the plots of the scattering intensity I vs the scattering vector q, where $q = (4\pi/\lambda)\sin(\theta/2)$, θ is the scattering angle, and λ is the wavelength of the incident X-ray. All of the testing membranes were prepared to be about 100 μm thick and exchanged into hydroxide form.

3. RESULTS AND DISCUSSION

3.1. Synthesis and Characterization of Monomers. Two aromatic diols were used to synthesize poly(ether sulfone)s (PES)s. One was 4,4′-dihydroxyl-2,2′,6,6′-tetraphenyldiphenyl ether **1**, which was synthesized according to the procedures developed by our group previously.[28] The other one, 4,4′-dihydroxy-2,2′,6,6′-tetra(*p*-tolyl)diphenyl ether **4**, was prepared from 2,2′,6,6′-tetrabromo-4,4′-dinitrodiphenylether,[29] via Suzuki coupling, reduction, diazotization, and hydrolysis reaction as shown in Scheme 1. The ^{1}H NMR spectra of compounds **2**−**4** are shown in Figure 1. The singlet peak at δ 7.75 ppm is assigned to protons H_a locating on the ortho position to the nitro groups on compound **2**. Protons on tolyl substituents, H_b and H_c, which couple with each other, appear at δ 7.23 and 7.19 ppm as doublets, respectively. The singlet at δ 2.41 ppm is assigned to proton H_d of methyl group. The integral ratio of the protons (H_a:H_b:H_c:H_d = 1:2:2:3) is also consistent with the proton number of compound **2**. The chemical structure is further verified by the molecular ion peak in the EI mass spectrum of compound **2** (Figure S1). After reduction, the resonance singlet peak of proton H_a ortho to amino group moves to more shielded position at δ 6.00 ppm, whereas the doublets of H_b and H_c only shift slightly. A new peak assigned to the amino groups appears at δ 4.50 ppm. After the amino groups was converted to hydroxyl groups, the peaks of protons H_a to H_d remain at similar chemical shifts. The peak of amino groups disappears and the new peak assigned to the hydroxyl groups emerges at δ 8.85 ppm. The EI mass spectra of compounds **3** and **4** shown in Figure S1 also confirm the chemical structures.

3.2. Synthesis of Poly(ether sulfone)s, XPh and XMePh. Poly(ether sulfone)s, XPh and XMePh, were synthesized from aromatic diols and bis(4-fluorophenyl) sulfone by aromatic nucleophilic substitution as shown in Scheme 2. The compositions of the copolymers could be manipulated by the feed ratio of monomers. X stands for the mole percentage of monomer **1** or **4** based on diols used for XPh or XMePh, respectively, and was controlled at 30, 40, 50, and 60 mol %. The ^{1}H NMR spectra of XPh and XMePh and their GPC results are shown Figure 2 and Table 1. All peaks could be assigned correctly from their chemical shifts, integral ratios and coupling relationship. The chemical structures of XPh and XMePh are similar. Their proton peaks appeared at almost the same chemical shifts except the peaks from the tolyl substituents. When the substituents are phenyl groups, the peaks of H_B and H_D overlap with that of H_H (δ 7.35−7.45 ppm), whereas proton H_C locates at more shielded position at δ 7.31 ppm. When the substituents are *p*-tolyl groups, the peaks of protons H_b and H_c move to more shielded position at δ 7.21 ppm and overlap with each other. Furthermore, a new singlet with an integral ratio of 3.00 assigned to proton H_d of methyl groups rises at δ 2.42 ppm. The compositions were calculated by the integral values of protons H_F/H_J and H_f/H_j, which varied with polymer compositions. The ^{1}H−^{1}H COSY spectra of 30Ph and 30MePh (Figure S2) also support the assignments of the chemical structures.

Table 1. Structural Composition and GPC Results of XPh and XMePh

polymer	feed ratio (x %/y%)[a]	x (%)[b]	y (%)[b]	M_n (KDa)[c]	M_w (KDa)[c]	PDI[c]
30Ph	30/70	30.3	69.7	176	361	2.05
40Ph	40/60	40.2	59.8	210	303	1.44
50Ph	50/50	50.5	49.5	155	335	2.16
30MePh	30/70	30.7	69.3	255	545	2.13
40MePh	40/60	40.6	59.4	298	571	1.91
50MePh	50/50	50.2	49.8	269	541	2.01
60MePh	60/40	59.5	40.5	256	514	2.01

[a]Monomer feed ratio in mol %. [b]x and y are the compositions in mol % of the repeating units derived from monomer **1**/monomer **4** and 4,4′-(hexafluoroisopropylidene)diphenol, respectively, determined by ^{1}H NMR spectra. [c]M_n: number-averaged molecular weight; M_w: weight-averaged molecular weight; PDI: polydispersity index: M_w/M_n.

As listed in Table 1, the compositions of XPh and XMePh calculated from proton NMR spectra are in good agreement with the corresponding feed ratio of monomers. In addition, XPh and XMePh were synthesized with high molecular weights and reasonable polydispersity index (Table 1). The number-averaged molecular weights of XPh and XMePh are in the range of 155−210 kDa and 255−298 kDa, respectively. It is quite important that even though high molecular weights could be essential to excellent mechanical properties of membranes, which is a critical factor associated with the performance of fuel cell, the processability of polymers (namely, solubility) in the following chemical reactions has also to be considered. Therefore, it is the reason that 4,4′-(hexafluoroisopropylidene)diphenol was used as comonomer. It is considered as a flexible segment and is beneficial to

https://dx.doi.org/10.1021/acsaem.0c02734
ACS Appl. Energy Mater. 2021, 4, 2201−2217

Scheme 3. Functionalization of XPh and XMePh

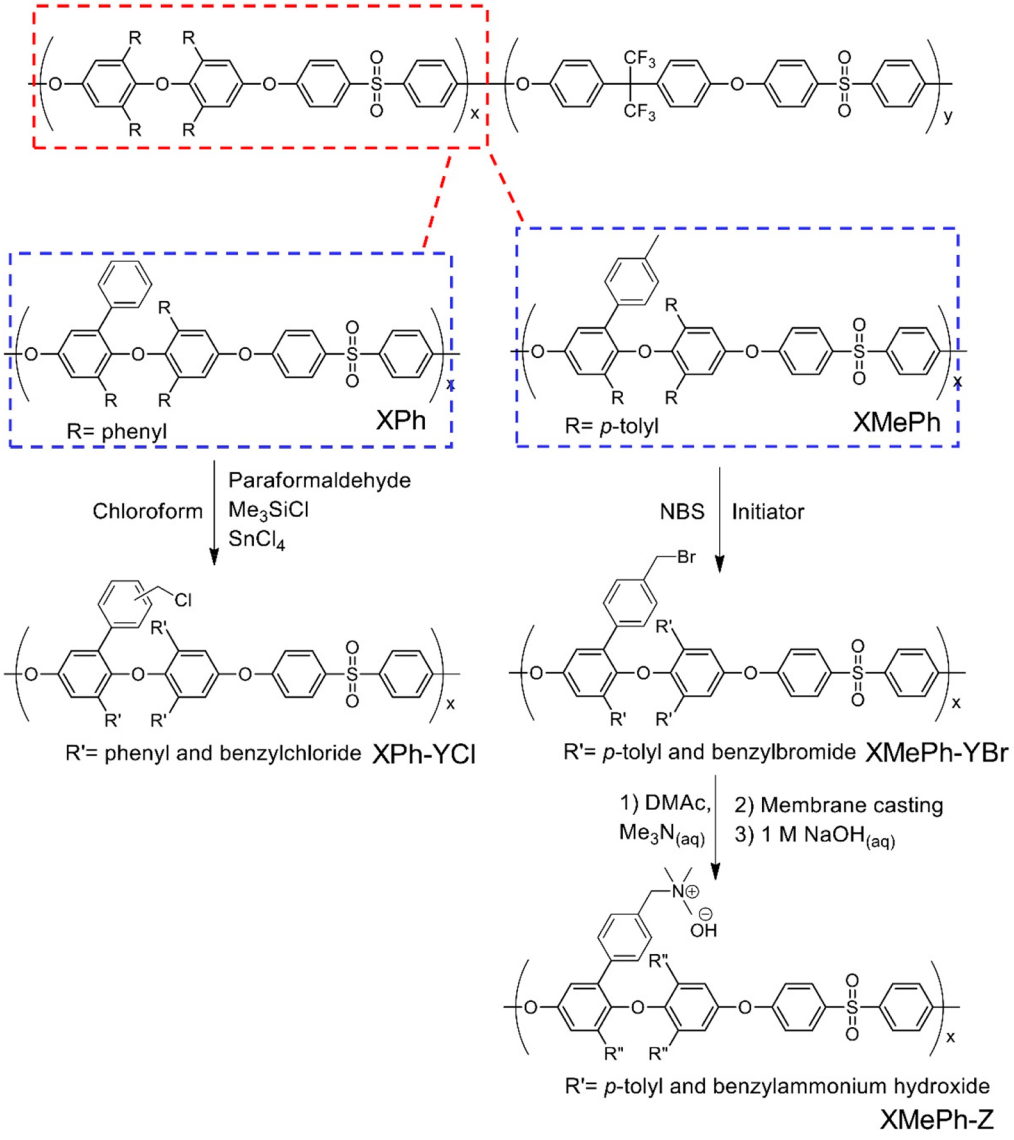

polymer solubility. In addition, its hydrophobic trifluoromethyl groups might also facilitate the phase separation between hydrophilic and hydrophobic segments.

3.3. Functionalization of XPh and XMePh. Initially, we attempted to introduce ionic groups selectively on the phenyl side groups of XPh by chloromethylation followed by quaternization reaction as shown in Scheme 3. Even though the carcinogenic chloromethyl methyl ether commonly used as the chloromethylation reagent has been replaced by paraformaldehyde and chlorotrimethylsilane with $SnCl_4$ as catalyst, the reaction still needs good control on polymer concentration and the amount of the reagents. Side reactions, including (1) polymer cross-linking resulted from Friedel–Crafts alkylation between an active phenyl ring and the chloromethyl group attached on another phenyl ring and (2) polymer degradation resulted from the cleavage of ether linkages by the attack of Lewis acids, have been recognized in previous article.[30]

Table 2 lists the reaction parameters of chloromethylation, degree of substitution (DS) and molecular weights of formed polymer. Chloromethylation was carried out at 60 °C in a sealed flask. According to our previous results, polymers should be added into the flask after paraformaldehyde dissolved completely to form electrophilic species.[30] By doing so, we hope that polymer chain scission could be avoided. In entry 1–3, polymer 40Ph with number-averaged molecular weight of 210 kDa was used. Even though the number-averaged molecular weights of the resulted polymers could be maintained at greater than 157 kDa after chloromethylation, the degrees of substitution are only 0–0.21 chloromethyl groups per repeating unit containing monomer **1**, which might lead to very low IEC values after the quaternization reaction. In entries 4–6, polymer 50Ph with number-averaged molecular weight of 155 kDa was used. The amount of stannic chloride was increased slightly and reaction time was prolonged to 48 h. However, the results were even worse. In entry 4, the resulting polymer possessed high molecular weight but no chloromethyl group was attached. When the amount of stannic chloride was further increased (entry 5 and 6), precipitates formed during the reaction, which implied that cross-linking reaction occurred. The low molecular weight of the dissolved portion of polymer (entry 5, with number-averaged molecular weight

https://dx.doi.org/10.1021/acsaem.0c02734
ACS Appl. Energy Mater. 2021, 4, 2201–2217

Table 2. Reaction Parameters of Chloromethylation, Degree of Substitution (DS), and Molecular Weight

entry	$(CH_2O)_n$/Me_3SiCl/$SnCl_4$ (mol/mol)[a]	polymer conc. (w/v%)	time (h)	DS[b]	M_n (KDa)	PDI
1[c]	10/10/0.1	2	24	0	174	1.79
2[c]	10/10/0.5	2	24	0.06	157	1.68
3[c]	10/10/2	2	24	0.21	202	2.12
4	10/10/0.5	2	48	0	147	2.02
5[d]	10/10/1	2	48	0.06	45	1.64
6[e]	10/10/2	2	48			
7[e]	50/50/2	0.5	48	0.47/0.58[g]	68	1.93
8[f]	50/50/2	0.5	96	0.17/0.60	85	1.93
9[f]	100/100/2	0.5	48	0.14/0.72	100	2.36
10[f]	300/300/2	0.5	48	0.49/1.32	86	1.96
11[f]	300/300/5	0.5	48	1.17/1.18	43	2.76

[a]mol mol^{-1}: moles per mole of repeating unit containing monomer **1**. [b]Number of substituted chloromethyl groups per repeating unit derived from monomer **1**. [c]40Ph was used in entries 1−3; 50Ph was used in other entries. Their molecular weights are listed in Table 1. [d]The product was partially soluble in the eluent of GPC and NMR solvent ($CDCl_3$). The data refers only to the soluble part of the polymer. [e]The product was totally insoluble. [f]A little solid suspension formed during the reaction in entry 7 and 8; obvious solid precipitate formed with yields of 37, 66, and 75% during the reaction in entry 9, 10, and 11, respectively. [g]Number of chloromethyl groups on side chain/main chain per repeating unit derived from monomer **1**.

of 45 kDa only) indicated severe polymer chain scission. Therefore, the concentration of polymer solution was decreased from 2 to 0.5% (w/v) in entries 7−11 to suppress the cross-linking reaction. The amounts of chloromethylation reagents, paraformaldehyde, and chlorotrimethylsilane were increased to promote the formation of electrophilic species as well. Nevertheless, the cross-linking phenomenon and polymer chain scission still occurred. Moreover, as the degree of substitution increased with the increased amount of chloromethylation reagents, two multiplet peaks corresponding to methylene protons appeared in the ^1H NMR spectra as shown in Figure S3. This indicates that chloromethylation might have taken place not only at the side phenyl groups. The chemical shift of methylene protons of chloromethylated side phenyl groups would appear around δ 4.70 ppm, whereas the multiplet appeared around δ 4.20 ppm might be resulted from the chloromethyl groups attached to phenyl rings adjacent to the ether linkage on the main chain. To avoid polymer chain scission, suppress cross-linking, and precisely control the attached positions of chloromethyl groups, we synthesized monomer **4** and the derived XMePh. Chloromethylation was thus skipped to avoid polymer degradation. Instead, radical-initiated bromination on benzylic position followed by quarternization was used to ensure the ionic sites were exclusively on the side phenyl groups.

Scheme 3 shows the functionalization of XMePh. Bromination was triggered by N-bromosuccinimide (NBS) and benzoyl peroxide (BPO, radical initiator) exclusively on the benzylic position of side groups. The reaction parameters of bromination, degree of substitution (DS), and molecular weight of polymers are listed in Table 3. The ^1H NMR spectra of the brominated 60MePh are shown in Figure S4. The degree of substitution is calculated by the integral values of aromatic proton adjacent to sulfone linkage and the protons on bromomethyl group. The temperature of bromination was

Table 3. Reaction Parameters, Degree of Substitution (DS), and Molecular Weight of Brominated 60MePh

entry[a]	NBS (mol/mol)[b]	T (°C)	time (h)	M_n (KDa)	PDI	DS[c]
1	2.00	85	8	65	1.70	2.08
2	1.20	85	8	73	1.81	3.20
3	1.20	60	8	78	1.70	0.84
4	1.20	60	20	65	1.74	3.46
5	1.05	60	36	67	1.62	0.94
6[d]	1.20	60	20	133	1.89	1.98

[a]The concentration of 60MePh in the solvent was fixed at 2.5% (w/v); the feed amount of BPO was 5 mol % of NBS. The original molecular weight Mn: 256 K Da, PDI: 2.01(Table 1). [b]mol/mol: moles per mole of methyl group. [c]Number of substituted bromomethyl groups per repeating unit derived from monomer **4**. [d]The feed amount of BPO was 2 mol % of NBS in entry 6.

controlled at 85 °C in entry 1 and 2 (Table 3). If all methyl groups in polymers were brominated into bromomethyl groups, the degree of substitution (DS) would be 4. Entry 1 with more NBS (2.0 mol/per mole of methyl group) has a DS of 2.08, whereas entry 2 with less NBS (1.2 mol/mol) had a higher DS of 3.20. And the proton peak of the methyl group, H_d, totally disappeared in entry 1. A deshielded peak at 7.65 ppm was observed for both entry 1 and 2, which indicated the formation of dibromomethyl group resulted from over bromination.[31] From the peak intensity of this dibromomethyl group, it indicated that over bromination was more severe in entry 1 than in entry 2. Because the degree of substitution is determined from the integral values of bromomethyl group, entry 2 with less NBS and thus fewer dibromomethyl groups showed higher degree of substitution than entry 1. This deshielded peaks was also observed in entry 4. These results suggested that over bromination would occur if the amount of NBS was excessive at 85 °C for 8 h (entry 1 and 2) or at 60 °C for 20 h (entry 4). The reaction temperature was then decreased to 60 °C, but the degree of substitution was quite low if the reaction was stopped in 8 h (entry 3). To prevent over bromination in entry 4, the amount of NBS was further decreased to 1.05 mol per mole of methyl group in entry 5, and the reaction was prolonged to 36 h. However, the degree of substitution in entry 5 also decreased to 0.94. Furthermore, less radical initiator BPO was used in entry 6, where only half methyl groups were brominated. In addition, the molecular weight also decreased in each entry, which suggests that the polymer chain was attacked by radicals at reaction temperature.

Therefore, a photoinitiator, (2,4,6-trimethylbenzoyl)-diphenyl-phosphine oxide (TPO), was chosen to replace BPO. We hope that polymer main chain scission can be minimized by using the photoinitiator under UV radiation (254 nm) at room temperature. The reaction parameters, degree of substitution (DS) and molecular weight of brominated XMePh are listed in Table 4. It was found that polymer main chain scission still happened, but only slightly. The DS values were higher and could be controlled accurately. For example, the DSs of all XMePhs are about 3.00 when 1.1 mol of NBS per mole of methyl groups were fed into the reaction mixture. In addition, the molecular weights of brominated polymers all remained higher than 139 kDa. Because DS is defined as the number of bromomethyl groups per tetra-*p*-tolyl (monomer **4**) containing repeating unit (the maximum DS is 4 for complete bromination), the ion exchange capacity (IEC) can be controlled not only by the DS but also

https://dx.doi.org/10.1021/acsaem.0c02734
ACS Appl. Energy Mater. 2021, 4, 2201−2217

Table 4. Reaction Parameters, Degree of Substitution (DS), and Molecular Weight of Brominated XMePh

entry[a]		polymer	NBS (mol/mol)[b]	M_n (KDa)	M_w (KDa)	PDI	DS[c]
30MePh	1	30MePh-3.00Br	1.10	180	354	1.97	3.00
	2	30MePh-3.20Br	1.30	213	377	1.81	3.20
	3	30MePh-3.72Br	1.50	174	350	2.01	3.72
40MePh	1	40MePh-2.96Br	1.10	148	270	1.82	2.96
	2	40MePh-3.40Br	1.30	162	308	1.89	3.40
	3	40MePh-3.72Br	1.50	159	298	1.87	3.72
50MePh	1	50MePh-3.00Br	1.10	220	452	2.05	3.00
	2	50MePh-3.32Br	1.30	289	551	1.91	3.32
	3	50MePh-3.84Br	1.50	240	483	2.01	3.84
60MePh	1	60MePh-2.64Br	0.80	162	325	2.01	2.64
	2	60MePh-3.00Br	1.10	155	273	1.76	3.00
	3	60MePh-3.40Br	1.30	139	258	1.85	3.40

[a]The concentration of XMePh in the solvent was fixed at 2.5% (w/v); the amount of TPO was 5 mol % of NBS. The original molecular weight is listed in Table 1. [b]mol/mol: moles per mole of methyl group. [c]Number of substituted bromomethyl groups, calculated according to the integral values in ^{1}H NMR spectra, per repeating unit containing monomer **4**.

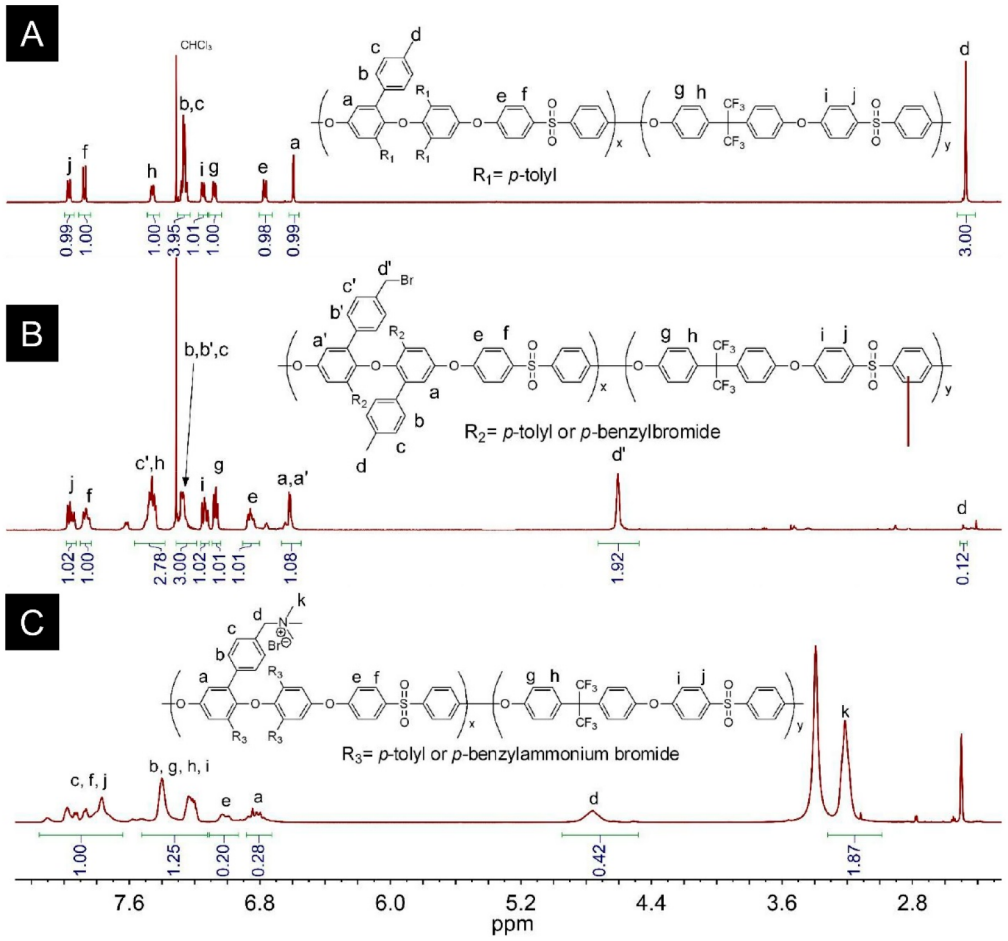

Figure 3. ^{1}H NMR spectra of (A) 50MePh ($CDCl_3$), (B) 50MePh-3.84Br ($CDCl_3$), and (C) 50MePh-1.99 (DMSO-d_6).

by the compositions of copolymers (X: the percentage of tetra-*p*-tolyl containing repeating unit in copolymer). After quaternization, bromomethyl groups were converted to cationic sites. For copolymers with the same composition, higher DS would lead to more and denser cationic groups. On the other hand, for copolymers with the same IEC values but different compositions, the copolymer with more tetra-*p*-tolyl containing repeating units (higher X value) would be brominated more dispersedly, thus leading to less densely located cationic groups.

3.4. Chemical Structure Identification of XMePh-YBr and XMePh-Z. The brominated copolymer and the corresponding quarternized ionomers are designated as XMePh-YBr and XMePh-Z, respectively, where X is the mole percent of diol monomer 4, Y is the degree of substitution (DS) in tetra-p-tolyl containing a repeating unit and Z is the IEC value determined by titration. 50MePh-

https://dx.doi.org/10.1021/acsaem.0c02734
ACS Appl. Energy Mater. 2021, 4, 2201−2217

Table 5. Ion Exchange Capacities (IECs), Water Uptake (WU), Dimensional Change, and Hydroxide Conductivity (σ) at 80 °C of XMePh-Z

entry	polymer	IEC_{NMR}[a] (mmol/g)	$IEC_{titr.}$[b] (mmol/g)	WU[b] (%)	TC[b] (%)	LC[b] (%)	σ at 80 °C[c] (mS/cm)
1	30MePh-1.23	1.21	1.23	42	6	6	13
2	30MePh-1.24	1.28	1.24	43	8	7	17
3	30MePh-1.44	1.41	1.44	50	9	15	26
1	40MePh-1.49	1.47	1.49	51	9	14	26
2	40MePh-1.59	1.64	1.59	61	14	16	30
3	40MePh-1.72	1.76	1.72	70	17	20	36
1	50MePh-1.70	1.72	1.70	68	16	18	31
2	50MePh-1.81	1.86	1.81	80	22	23	36
3	50MePh-1.99	2.07	1.99	91	28	25	44
1	60MePh-1.61	1.75	1.61	68	18	25	22
2	60MePh-1.95	1.93	1.95	120	28	28	33
3	60MePh-2.07	2.11	2.07	130	35	33	45

[a]Ion exchange capacity was determined by ^{1}H NMR spectrum and titration, respectively. [b]WU: water uptake; TC and LC: thickness change and length change in percentage after ion exchange, respectively. [c]Hydroxide conductivity at 98%RH and 80 °C.

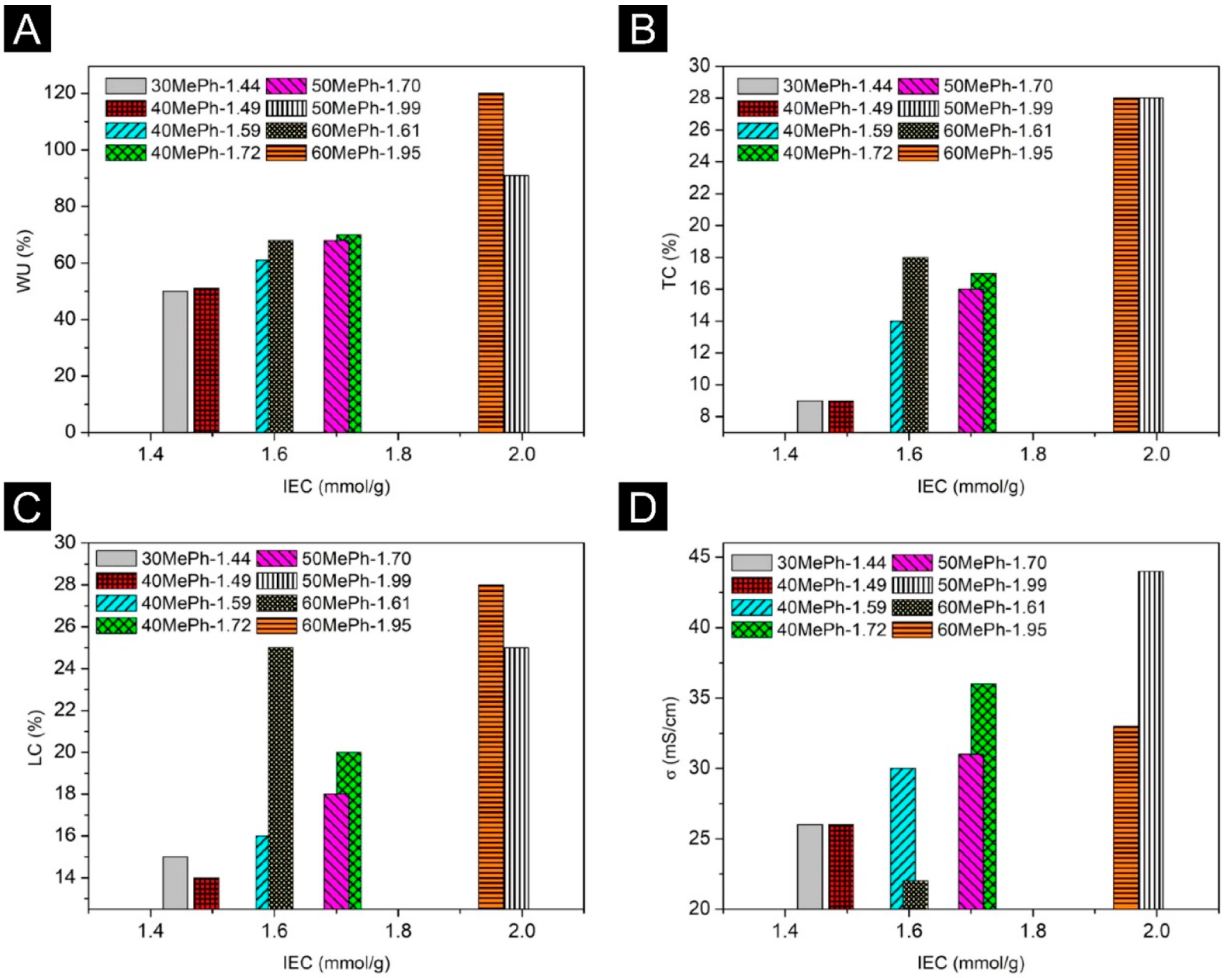

Figure 4. Relationship of (A) water uptake, (B) thickness change, (C) length change, and (D) hydroxide conductivity at 80 °C versus IEC values.

3.84Br and the corresponding 50MePh-1.99 are taken as the examples to illustrate the chemical structure identification. Their ^{1}H NMR spectra as well as that of 50MePh are shown in Figure 3. The peak appearing at δ 4.56 ppm is assigned as proton "$H_{d'}$" of bromomethyl groups with an integral value of 1.92. The degree of substitution can be calculated by the following equation: DS = $(I_{d'}/2)/(I_f/4)$, where $I_{d'}$ and I_f refer to the integral values of "$H_{d'}$" and "H_f" of 50MePh-3.84Br, respectively. Relatively, the integral value of proton "H_d" of 50MePh decreased from 3.00 to 0.12. The amount of residual methyl groups could also be calculated as 0.16 per repeating unit derived from monomer **4**. Other aromatic protons of 50MePh-3.84Br appeared at chemical shifts similar to those of 50MePh except proton "H_c". As shown in Figure S5 (^{1}H−^{1}H COSY spectrum), the peak at δ 7.43 ppm coupled with the peaks at δ 7.24 (H_b, H_b', H_c) and 7.03 (H_g) ppm

https://dx.doi.org/10.1021/acsaem.0c02734
ACS Appl. Energy Mater. 2021, 4, 2201−2217

simultaneously, which indicates that proton "$H_{c'}$" overlapped with proton "H_h". The quaternization reaction was carried out at room temperature for 2 days. After the bromomethyl groups were quaternized with trimethylamine via Menshutkin reaction, the peaks became broad. The degree of quaternization (DQ) still could be estimated according to the integral values of "H_d" and "H_k" of 50MePh-1.99. If all bromomethyl groups were converted to trimethylammonium groups, the integral ratio of "H_k" relative to "H_d" would be close to 4.5. The degrees of quaternization was determined to be quantitative in all cases of XMePh-Z. Thus, the IEC_{NMR} of the resulted XMePh-Z was estimated based on the degrees of bromination.

3.5. Characterization of Membrane Properties. *3.5.1. Ion Exchange Capacity (IEC), Water Uptake, Dimensional Change, and Hydroxide Conductivity.* Ion exchange capacity (IECs), water uptake, dimensional change, and hydroxide conductivity at 80 °C of XMePh-Z are listed in Table 5. All XMePh-Z are derived from the corresponding brominated XMePh listed in Table 4. For example, 30MePh-1.23, 30MePh-1.24, and 30MePh-1.44 were the products in entry 1−3 of 30MePh in Table 4, respectively. Ion exchange capacity (IEC) is defined as the mmole number of cationic groups per gram of dry polymer. It is a crucial factor related to water uptake and hydroxide conductivity. In Table 5, IEC values determined by NMR spectra (IEC_{NMR}) and titration ($IEC_{titr.}$) are very close, indicating the quantitative conversion of quarternization and completion of anion exchange from bromide to hydroxide. If the copolymer compositions are the same, water uptake, dimensional change (in thickness TC and in length LC directions) and hydroxide conductivity increased as more cationic groups were present in the membranes. In general, an AEM possessing higher IEC and water uptake could transfer hydroxide ion more efficiently because of high concentration of ionic sites and facile dissociation of ionic pairs based on Grotthuss mechanism.[12]

As mentioned previously, the IEC values of XMePh-Z can be manipulated by controlling copolymer compositions and different degrees of bromination. It also means that it is possible to prepare AEMs with the same IEC but different distribution of cationic groups tethered on polymer chain. For example, 40MePh-1.72 and 50MePh-1.70 having similar IEC values were derived from the corresponding 40MePh-3.72Br and 50MePh-3.00Br with different bromination degree, respectively. The cationic groups of 40MePh-1.72 supposedly located more densely together than those of 50MePh-1.70. Different distribution of cationic groups in AEMs with similar IEC values may exhibit distinct properties. Figure 4 shows the relationship of water uptake, dimensional change and hydroxide conductivity at 80 °C versus IEC values with different distribution of cationic groups. In Figure 4A, when IEC values are less than 1.90 mmol/g, the water uptake seems independent of the distribution of cationic groups. However, when the IEC values are higher than 1.90 mmol/g, 50MePh-1.99 with denser cationic groups absorbed less water (WU = 91%) than 60MePh-1.95 (WU = 120%). In Figure 4B, C, 60MePh-1.95 swelled more (LC = 28%) than 50MePh-1.99 (LC = 25%) in length direction but swelled equally in thickness direction. Furthermore, 40MePh-1.59 and 60MePh-1.61, whose variation in the distribution of cationic groups is larger, possessed similar water uptake, but the dimensional change of 60MePh-1.61 (LC = 25%, TC = 18%) is much larger than that of 40MePh-1.59 (LC = 16%, TC = 14%) especially in length direction. Large swelling of membrane leads to excessive deformation, which is detrimental to the fabrication of membrane electrode assemblies and to the durability of fuel cells as well. In Figure 4D, except 30MePh-1.44 and 40MePh-1.49, other AEMs tethered with denser distribution of cationic groups exhibited higher hydroxide conductivity at 80 °C. For example, the hydroxide conductivity of 60MePh-1.95 (33 mS/cm) is less than that of 50MePh-1.99 (44 mS/cm) even though 60MePh-1.95 absorbed more water than 50MePh-1.99. Moreover, the hydroxide conductivity of 60MePh-1.61 is even lower than those of 30MePh-1.44, 40MePh-1.49, and 40MePh-1.59, whose water uptakes are less. This could be a result of the severe dimensional change of 60MePh-1.61, leading to the dilution of cationic groups per unit volume. From these comparisons, it indicated that AEMs tethered with cationic groups more closely together could absorb less water, show lower dimensional change, and exhibit higher hydroxide conductivity.

The hydroxide conductivity of membranes is also dependent on temperature and relative humidity, in addition to IEC and water uptake. Figure 5A shows hydroxide conductivity of 30MePh-1.44, 40MePh-1.72, 50MePh-1.99 and 60MePh-2.07 from 40 to 80 °C. To exclude the contamination of CO_2 from the formation of carbonate and bicarbonate, the measurements were carried out in an oven filling with N_2. Their hydroxide conductivity increased as temperature was raised. For instance, the hydroxide conductivity of 50MePh-1.99 increased from 19

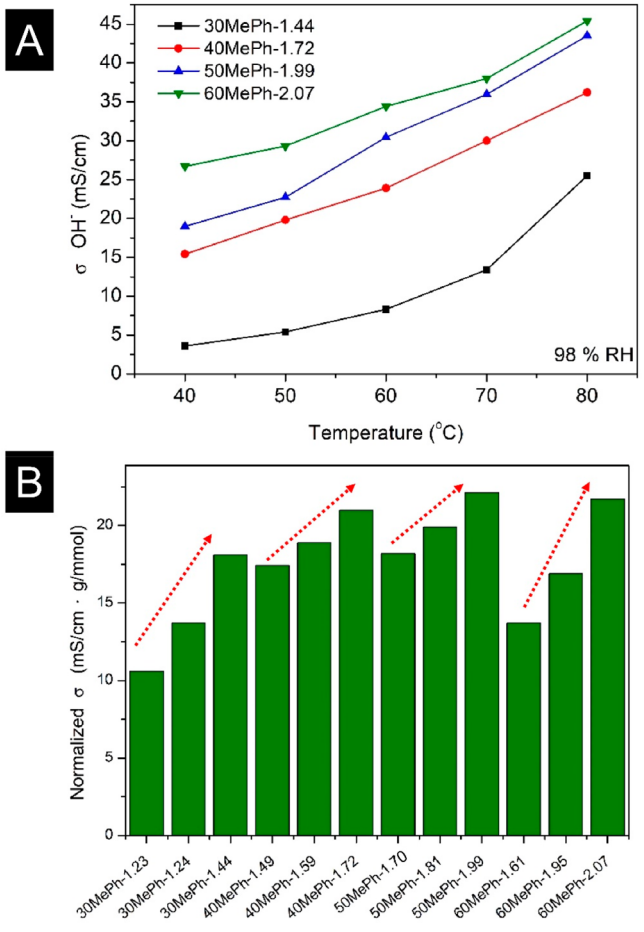

Figure 5. (A) Hydroxide conductivity at temperature from 40 to 80 °C and (B) normalized hydroxide conductivity at 80 °C.

https://dx.doi.org/10.1021/acsaem.0c02734
ACS Appl. Energy Mater. 2021, 4, 2201−2217

to 44 mS/cm as the temperature was raised from 40 to 80 °C. If we normalized the hydroxide conductivity with the corresponding IEC (hydroxide conductivity divided by IEC as shown in Figure 5B), the contribution to hydroxide conductivity per cationic site is higher when the IEC values of copolymers with the same copolymer compositions were higher. On the other hand, each cationic group of AEMs with similar IEC values and denser cationic groups contributes more to hydroxide conductivity (for example, 40MePh-1.72, 50MePh-1.70, and 10Meph-1.59, 60MePh-1.61 in Figure 5 B).

3.5.2. Thermal Stability and Mechanical Strength. The thermal degradation temperature (T_d) and glass transition temperature (T_g) of polymers were characterized by thermal gravimetric analysis (TGA) and differential scanning calorimetry (DSC), respectively. Table S1 lists the decomposition temperature at 5% weight loss ($T_{5\%}$), residual weight at 800 °C, and glass transition temperature of XMePh. The degradation curves of each XMePh were extremely similar. The $T_{5\%}$ and R_{w800} of XMePhs are in a range of 429−436 °C and 50−52 wt %. It seems that there is no significant difference in thermal degradation between these two repeating units. However, a steady growth of T_g can be recognized as the mole percent of repeating unit derived from monomer **4** increased. For example, 60MePh had a T_g of 232 °C, which is higher than that of 30MePh (208 °C). The results suggest that higher energy required for the movement of polymer segments containing repeating unit derived from monomer **4**. Figure 6

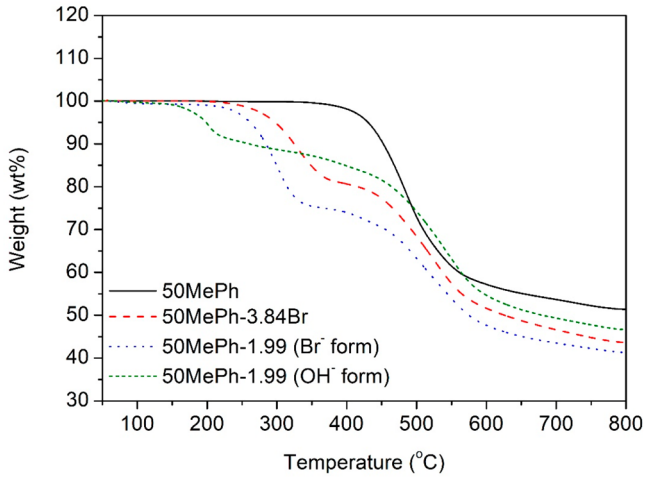

Figure 6. TGA thermograms of 50MePh and its derivatives.

shows the TGA thermograms of 50MePh and its functionalized derivatives, including 50MePh-3.84Br and the corresponding 50MePh-1.99 (in bromide and in hydroxide form). The $T_{5\%}$ of 50MePh was observed at 430 °C. 50MePh-3.84Br thermally degraded at 247 °C because of the decomposition of bromomethyl groups, then at 470 °C resulted from the degradation of polymer backbone. The first degradation of 50MePh-1.99 in Br^- form occurred at 210 °C, revealing that the trimethylammonium bromide was less stable than bromomethyl group. After the bromide was replaced by hydroxide, 50MePh-1.99 in OH^- form decomposed initially at 155 °C. The thermal stability of 50MePh-1.99 in OH^- form is still high enough to sustain the conditions of fuel cell operation at 50−80 °C.

The mechanical properties, including tensile strength, strain at break and Young's modulus of 30MePh-1.44, 40MePh-1.72, 50MePh-1.99, and 60MePh-2.07 membranes, are listed in Table 6. Their stress−strain curves are also shown in Figure S6

Table 6. Mechanical Properties of 30MePh-1.44, 40MePh-1.72, 50MePh-1.99, and 60MePh-2.07 Membranes

polymer	ion form	strength (MPa)[a,b]	strain (%)[a,b]	Young's modulus (GPa)
30MePh-1.44	Br^- (dry)	31	31	1.07
	OH^-(wet)	21	65	0.72
40MePh-1.72	Br^- (dry)	28	53	1.11
	OH^-(wet)	18	83	0.48
50MePh-1.99	Br^- (dry)	27	72	1.01
	OH^-(wet)	13	91	0.29
60MePh-2.07	Br^- (dry)	25	51	1.03
	OH^-(wet)	6	18	0.22

[a]Measurements were conducted with a constant cross-head speed of 5 mm/min under ambient atmosphere. [b]Tensile strength and strain at break.

in Supporting Information. Membranes in bromide form (dry) had the tensile strength, strain at break and Young's modulus in the ranges of 25−31 MPa, 31−72%, and 1.01−1.11 GPa, respectively. In contrast, membranes in OH^- form (wet) exhibited a tensile strength of 6−21 MPa, strain at break of 18−91%, and Young's modulus of 0.22−0.72 GPa. The tensile strength decreased with increased IEC values and water uptakes, whereas the strain increased with increased IEC values except that of 60MePh-2.07. The strain of 60MePh-2.07 in the OH^- form is only 18%. On the other hand, 40MePH-1.72 in OH^- form exhibited excellent mechanical properties, with a tensile strength of 18 MPa, strain of 83%, and Young's modulus of 0.48 GPa.

3.5.3. Membrane Morphology. The microstructure of membranes was investigated by atomic force microscope and scanning electron microscope as shown in Figure 7 and Figure S7, respectively. The correlation between height and phase of AFM images can be excluded, which indicates that the roughness of membrane surface did not interfere with the phase image. The surface roughness of all membranes are less than ±2 nm, showing high flatness of the membrane surface. In the phase images, if nanophase separation is formed, the distinction of dark and bright regions will be observed, which originate from the soft blocks of hydrophilic quaternary ammonium and rigid blocks of hydrophobic main chain segments, respectively. Only a few isolated dark regions with diameters of 9−16 nm appeared in the phase image of 30MePh-1.44, whereas dark regions become much larger (26−40 nm) in the phase image of 40MePh-1.72. However, the soft blocks are still separated and distribute unevenly. The distribution of dark regions (25−35 nm) becomes more regular and continuous in the phase image of 50MePh-1.99. The transition of membrane morphology between 30MePh-1.44, 40MePh-1.72, and 50MePh-1.99 is attributed to the increase in cationic groups existing in the membranes. However, the dark regions (15−25 nm) of 60MePh-1.95 are smaller than those of 50MePh-1.99. This might be a result of more densely located cationic groups of 50MePh-1.99 than those of 60MePh-1.95. Larger and continuous domains of hydrophilic cationic groups can boost the transport of hydroxide. The difference in microstructures between 50MePh-1.99 and 60MePh-1.95 can explain that the hydroxide

https://dx.doi.org/10.1021/acsaem.0c02734
ACS Appl. Energy Mater. 2021, 4, 2201−2217

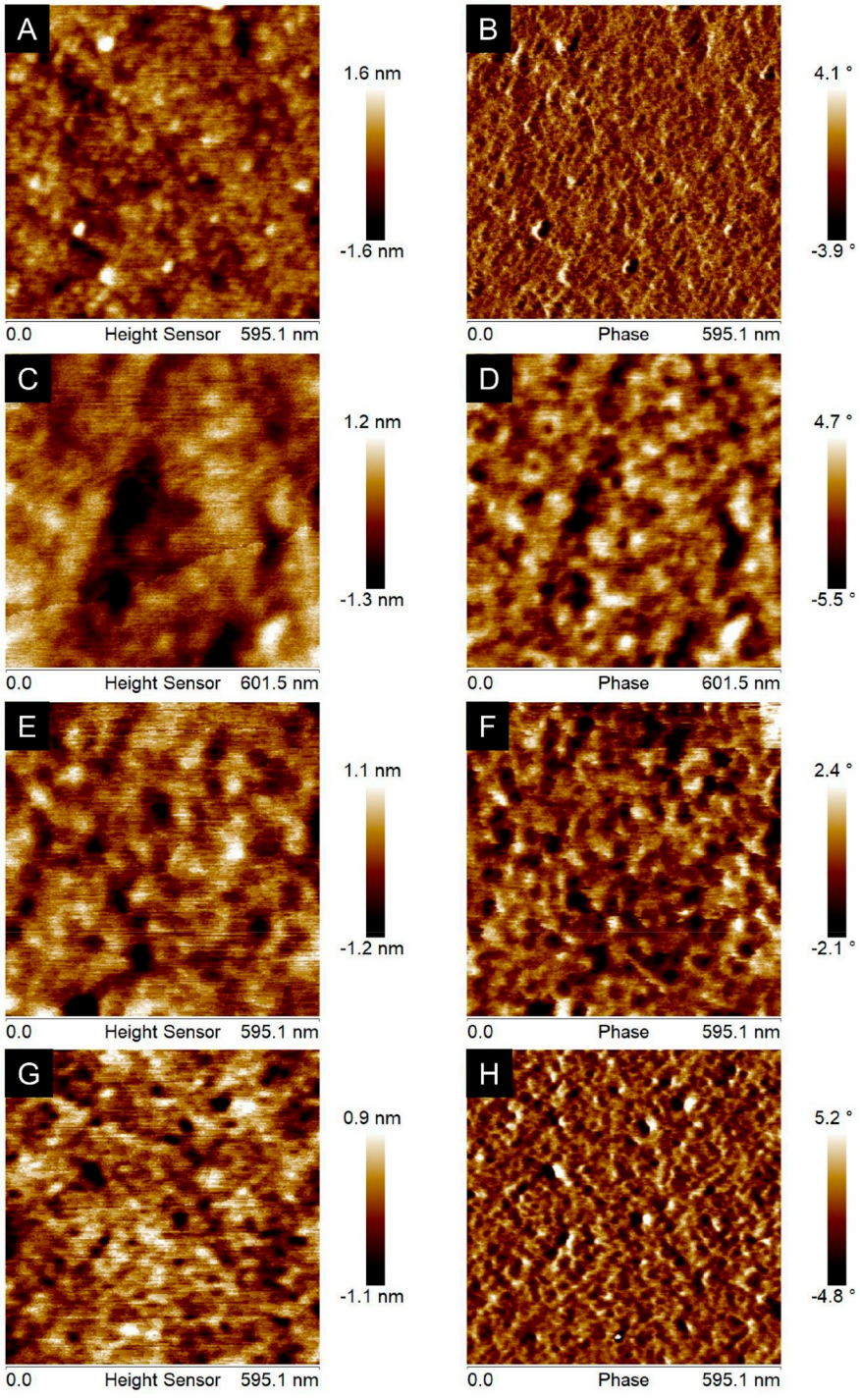

Figure 7. Height and phase AFM images of (A, B) 30MePh-1.44, (C, D) 40MePh0−1.72, (E, F) 50MePh-1.99 and (G, H) 60MePh-1.95 membranes.

conductivity of 50MePh-1.99 is higher than that of 60MePh-1.95 even though their IEC values are similar.

More evidence regarding the nanophase separation can be found from small-angle X-ray diffraction (SAXS) investigation. Figure 8 shows SAXS profiles of 50MePh-1.70 and 50MePh-1.99. No scattering peak was observed from 50MePh-1.70. By contrast, 50MePh-1.99 has a distinct peak at q = 1.12 nm^{-1}. The distance between ionic clusters of 50MePh-1.99 is 5.63 nm determined by Bragg's law. Combined with the results shown in Figure 4, it makes perfect sense that 50MePh-1.99 with denser distribution of ionic groups, formed percolating channels of clustered ionic groups, thus exhibited higher hydroxide conductivity at lower water uptake than 60MePh-1.95 with similar IEC values. From the results shown in Figure 4, 50MePh-1.70 exhibited lower hydroxide conductivity than 40MePh-1.72 containing denser distribution of ionic groups with similar IEC value. No diffraction peak was observed for 50MePh-1.70, indicating no significant amount of ionic clusters was formed.

The SEM images (Figure S7) of surface and cross section of 40MePh-1.72 and 50MePh-1.99 membranes displayed a dense and nonporous morphology. A dense membrane can effectively

https://dx.doi.org/10.1021/acsaem.0c02734
ACS Appl. Energy Mater. 2021, 4, 2201−2217

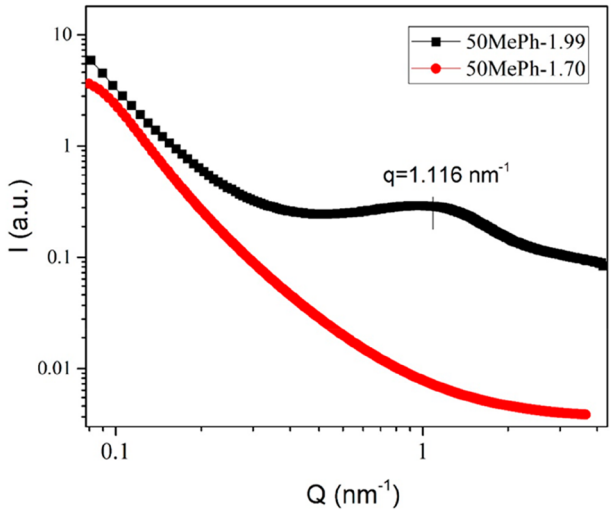

Figure 8. SAXS profiles of 50MePh-1.70 and 50MePh-1.99.

separate gases and prevent fuel crossover, which is necessary for high open circuit voltage during fuel cell operation.[32−34]

3.5.4. Alkaline Stability. In addition to hydroxide conductivity, the stability of membranes under an alkaline environment is also a crucial issue. For the purpose of evaluation on alkaline stability, membranes were immersed in a 1.0 M NaOH aqueous solution at 60 °C for a certain period of time up to 720 h. The samples were taken out and washed with deionized water. The IEC values and hydroxide conductivity of membranes were then measured. The alkaline stability was evaluated by the changes in IEC values and hydroxide conductivity after the immersion. Figure 9 shows the alkaline

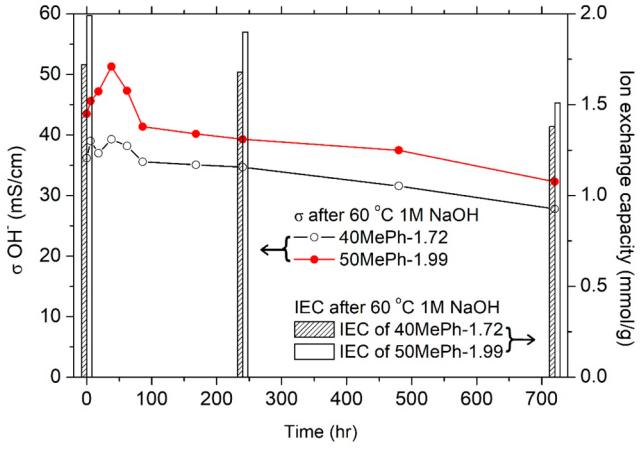

Figure 9. Alkaline stability of 40MePh-1.72 (black symbols) and 50MePh-1.99 (red symbols) in terms of hydroxide conductivity measured at 80 °C and 98%RH (line) and IEC (bar).

stability of 40MePh-1.72 and 50MePh-1.99, where the columns represent IEC values, and the lines represent hydroxide conductivity. The hydroxide conductivity of both 40MePh-1.72 and 50MePh-1.99 rose slightly in the initial 86 h of the immersion. It is likely due to the incomplete ion exchange even though the period of ion exchange procedure continued at room temperature for 3 days. In contrast, the hydroxide conductivity started to decay after 100 h of immersion. After 720 h of immersion, the hydroxide conductivity of 50MePh-1.99 reduced from 44 to 32 mS/cm (73% retention) and the IEC value declined from 1.99 to 1.51 mmol/g (76% retention). In the case of 40MePh-1.72, the hydroxide conductivity and IEC were 28 mS/cm (78% retention) and 1.38 mmol/g (81% retention), respectively, after 720 h of alkaline stability test. There are only α carbons of trimethylammonium cations existing in repeating units, so the degradation of cations can only occur by the attack by hydroxide via nucleophilic substitution.[9] Polymer main chain degradation by the hydroxide attack on ether linkage is also documented.[20] The results also showed that membranes with lower IEC values exhibited better alkaline stability. It is might be due to the fact that the low water uptake resulted from low IEC values might deter the attack from hydroxide in the alkaline solution. Further improvement on alkaline stability might be achieved by cross-linking the membranes and by adjusting IEC values to a lower level.

The mechanical properties of 40MePh-1.72 and 50MePh-1.99 membranes after alkaline stability test (1.0 M NaOH at 60 °C, 720 h) were measured (Table S2). We found that the membranes maintained their physical appearance, but the performance decayed. Their tensile strength decreased around 37%, tensile strain around 14%, and Young's modulus 30%.

To further investigate alkaline stability, we used ^{1}H NMR to verify whether polymer backbone or cationic groups degraded. Figure S8 showed the ^{1}H NMR spectra of 50MePh-1.99 membranes before and after alkaline stability test for 5 days. There is no obvious change between the aromatic and methyl group. The decay, represented by the peak area of methylene group (H_d, 4.50−4.70 ppm) relative to that of aromatic hydrogen b, g, h, and i (7.10−7.50 ppm), is only 97.2%. It matches well with the decay in IEC value after alkaline stability test for 5 d (Figure 9). The membrane of 50MePh-1.99 still remained their physical appearance. It can be assumed that the decay in IEC values should mainly result from the degradation of methylene-group-bearing quaternary ammonium cations in the first 5 days of the alkaline stability test.

3.5.5. Fuel Cell Performance. The membrane electrode assembly (MEA) of 40MePh-1.72 was prepared by sandwiching a catalyst-coated membrane between two pieces of carbon paper. The polarization and power density curves are shown in Figure 10. Their open circuit voltages (OCVs), maximum power density, and current density at 0.2 V are listed in Table 7. The MEA of commercial FAA-3 membrane was also

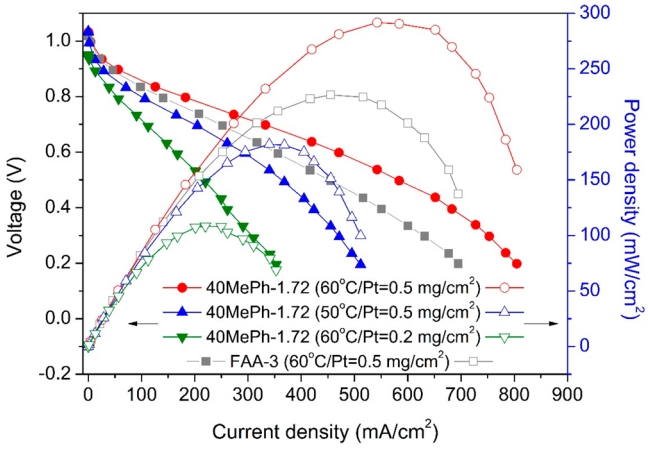

Figure 10. Polarization and power density curves of AEMFCs based on 40MePh-1.72.

https://dx.doi.org/10.1021/acsaem.0c02734
ACS Appl. Energy Mater. 2021, 4, 2201−2217

Table 7. Fuel Cell Performance

membrane	T (°C)	Pt loading (mg/cm^2)	OCV (V)[a]	power density (mW/cm^2)[b]	current density (mA/cm^2)[c]
40MePh-1.72	60	0.5	1.03	291	805
40MePh-1.72	50	0.5	1.04	182	512
40MePh-1.72	60	0.2	0.94	108	353
FAA-3	60	0.5	1.02	226	695

[a]Open circuit voltage [b]Maximum power density. [c]Current density at 0.2 V.

prepared and tested as a comparison. The fuel cells were operated with H_2 and O_2 under 87 and 91% RH, respectively. The OCVs and maximum power density of fuel cells based on 40MePh-1.72 and FAA-3 were in the range of 0.94−1.04 V and 108−291 mW/cm^2, respectively. The high OCVs indicates that these membranes effectively separated H_2 and O_2 to prevent fuel crossover. In the case of 40MePh-1.72 with Pt loading of 0.2 mg/cm^2, the OCV was 0.94 V. The maximum power density (108 mW/cm^2) and current density (353 mA/cm^2) at 0.2 V were low due to low Pt loading. When the Pt loading was increased to 0.5 mg/cm^2, not only the OCVs were higher than 1.00 V, the power density could also be improved to 182 and 291 mW/cm^2 at 50 and 60 °C, respectively. In the case of fuel-cell-based on FAA-3, its OCV and maximum power density were 1.02 V and 226 mW/cm^2, respectively. The results of a fuel cell based on FAA-3 are comparable to the values reported by another group using the same Pt loading.[35] The fuel cell based on 40MePh-1.72 exhibited a higher maximum peak power density than that based on FAA-3 under the same test conditions.

The comparison with membranes based on polyethersulfones reported by other groups is shown in Table S3.[36−45] The test parameters might cause the differences in fuel cell performance. The operating condition of a single cell at 60 °C, 100%RH, and 0.5 mg/cm^2 of Pt loading seems to be mostly adopted, but it might not be the best condition for every single fuel cell. The maximum power density of reported AEMs based on polyethersulfones ranged from 29.5 to 260 mW/cm^2 among the results we collected from literature. In the case of 40MePh-1.72, the performance of a single fuel cell, reaching OCV of 1.03 V and maximum power density of 291 mW/cm^2, is higher than the general level.

However, it is still possible to further improve the performance of fuel cells by sophisticated optimization on the process parameters of MEA fabrication and test conditions. On the other hand, 50MePh-1.99 and 60MePh-2.07 membranes could not be employed in a fuel cell because of their weak mechanical strength and poor dimension stability in their wet conditions.

4. CONCLUSIONS

Poly(ether sulfone)s, XPh and XMePh, were successfully prepared from the monomer **1** and monomer **4**, respectively, via aromatic nucleophilic substitution polymerization. In our initial plan, XPh was to be functionalized with trimethylammonium hydroxide on the side phenyl groups through chloromethylation, quaternization and ion exchange reaction. However, the attempt failed because of severe polymer chain scission and no selectivity of reacted positions during chloromethylation. Therefore, XMePh was synthesized to avoid chloromethylation. The high selectivity on reaction position without polymer chain scission were achieved by photo initiated bromination on XMePh. The IEC values and distribution of ionic groups can be manipulated by the degree of bromination and various monomer ratios. Anionic exchange membranes tethered with cationic groups locating closely together seem to absorb less water but exhibit higher hydroxide conductivity. Obvious nanophase separation of membrane morphology leading to larger and continuous domains of hydrophilic cationic groups can be found that boosts the transport of hydroxide. These anionic exchange membranes also demonstrated good alkaline stability. In the case of 40MePh-1.72, the hydroxide conductivity and IEC remained at 78 and 81% of their original values, respectively, after 720 h of alkaline stability test. The single fuel cells based on 40MePh-1.72 using 0.5 mg/cm^2 of Pt loading exhibited a power density of 291 mW/cm^2 ,which is higher than that of commercially available FAA-3 under the same conditions.

■ ASSOCIATED CONTENT

Supporting Information

The Supporting Information is available free of charge at https://pubs.acs.org/doi/10.1021/acsaem.0c02734.

EI-mass spectra of compounds **2**, **3**, and **4**; ^{1}H−^{1}H COSY spectra of 30Ph and 30MePh; ^{1}H NMR spectra of chloromethylated 50Phs; ^{1}H NMR spectra of brominated 60MePh by using BPO as the initiator; ^{1}H−^{1}H COSY spectrum of 50MePh-3.00Br; strength−strain curves of 30MePh-1.44, 40MePh-1.72, 50MePh-1.99, and 60MePh-2.07 membranes; surface and cross-section SEM images of 40MePh-1.72 and of 50MePh-1.99; thermal stability of XMePh; ^{1}H NMR spectra of 50MePh-1.99 before and after alkaline stability test for 5 days; mechanical properties of membranes before and after alkaline stability test; comparison of fuel cell performance based on poly(ether sulfone)s (PDF)

■ AUTHOR INFORMATION

Corresponding Author

Jyh-Chien Chen − *Department of Materials Science and Engineering, National Taiwan University of Science and Technology, Taipei 10607, Taiwan;* orcid.org/0000-0002-8630-4966; Phone: +886 2 27376526; Email: jcchen@mail.ntust.edu.tw

Authors

Ping-Yen Chen − *Department of Materials Science and Engineering, National Taiwan University of Science and Technology, Taipei 10607, Taiwan*

Tse-Han Chiu − *Department of Materials Science and Engineering, National Taiwan University of Science and Technology, Taipei 10607, Taiwan*

Kai-Pin Chang − *Institute of Polymer Science and Engineering, National Taiwan University, Taipei 10617, Taiwan*

Shih-Huang Tung − *Institute of Polymer Science and Engineering, National Taiwan University, Taipei 10617, Taiwan;* orcid.org/0000-0002-6787-4955

Wei-Tsung Chuang − *National Synchrotron Radiation Research Center (NSRRC), Hsinchu Science Park, Hsinchu 30076, Taiwan;* orcid.org/0000-0002-9000-2194

Kuei-Hsien Chen − *Center for Condensed Matter Sciences, National Taiwan University, Taipei 10617, Taiwan;*

https://dx.doi.org/10.1021/acsaem.0c02734
ACS Appl. Energy Mater. 2021, 4, 2201−2217

Institute of Atomic and Molecular Science, Academia Sinica, Taipei 10617, Taiwan

Complete contact information is available at: https://pubs.acs.org/10.1021/acsaem.0c02734

Notes

The authors declare no competing financial interest.

REFERENCES

(1) Fenton, D. E.; Parker, J. M.; Wright, P. V. Complexes of alkali metal ions with poly(ethylene oxide). *Polymer* **1973**, *14*, 589.
(2) Hong, J. G.; Zhang, B.; Glabman, S.; Uzal, N.; Dou, X.; Zhang, H.; Wei, X.; Chen, Y. Potential ion exchange membranes and system performance in reverse electrodialysis for power generation: A review. *J. Membr. Sci.* **2015**, *486*, 71.
(3) Leong, J. X.; Daud, W. R. W.; Ghasemi, M.; Liew, K. B.; Ismail, M. Ion exchange membranes as separators in microbial fuel cells for bioenergy conversion: A comprehensive review. *Renewable Sustainable Energy Rev.* **2013**, *28*, 575.
(4) Vincent, I.; Bessarabov, D. Low cost hydrogen production by anion exchange membrane electrolysis: A review. *Renewable Sustainable Energy Rev.* **2018**, *81*, 1690.
(5) Ngai, K. S.; Ramesh, S.; Ramesh, K.; Juan, J. C. A review of polymer electrolytes: fundamental, approaches and applications. *Ionics* **2016**, *22*, 1259.
(6) Wang, Y.; Chen, K. S.; Mishler, J.; Cho, S. C.; Adroher, X. C. A review of polymer electrolyte membrane fuel cells: Technology, applications, and needs on fundamental research. *Appl. Energy* **2011**, *88*, 981.
(7) Zhang, H.; Shen, P. K. Recent Development of Polymer Electrolyte Membranes for Fuel Cells. *Chem. Rev.* **2012**, *112*, 2780.
(8) Zhang, H.; Shen, P. K. Advances in the high performance polymer electrolyte membranes for fuel cells. *Chem. Soc. Rev.* **2012**, *41*, 2382.
(9) Sun, Z.; Lin, B.; Yan, F. Anion-Exchange Membranes for Alkaline Fuel-Cell Applications: The Effects of Cations. *ChemSusChem* **2018**, *11*, 58.
(10) Pan, Z. F.; An, L.; Zhao, T. S.; Tang, Z. K. Advances and challenges in alkaline anion exchange membrane fuel cells. *Prog. Energy Combust. Sci.* **2018**, *66*, 141.
(11) Cheng, J.; He, G.; Zhang, F. A mini-review on anion exchange membranes for fuel cell applications: Stability issue and addressing strategies. *Int. J. Hydrogen Energy* **2015**, *40*, 7348.
(12) Merle, G.; Wessling, M.; Nijmeijer, K. Anion exchange membranes for alkaline fuel cells: A review. *J. Membr. Sci.* **2011**, *377*, 1.
(13) Varcoe, J. R.; Atanassov, P.; Dekel, D. R.; Herring, A. M.; Hickner, M. A.; Kohl, P. A.; Kucernak, A. R.; Mustain, W. E.; Nijmeijer, K.; Scott, K.; Xu, T.; Zhuang, L. Anion-exchange membranes in electrochemical energy systems. *Energy Environ. Sci.* **2014**, *7*, 3135.
(14) Li, Q.; Liu, L.; Miao, Q.; Jin, B.; Bai, R. Hydroxide-conducting polymer electrolyte membranes from aromatic ABA triblock copolymers. *Polym. Chem.* **2014**, *5*, 2208.
(15) Zhu, L.; Zimudzi, T. J.; Wang, Y.; Yu, X.; Pan, J.; Han, J.; Kushner, D. I.; Zhuang, L.; Hickner, M. A. Mechanically Robust Anion Exchange Membranes via Long Hydrophilic Cross-Linkers. *Macromolecules* **2017**, *50*, 2329.
(16) Jannasch, P.; Weiber, E. A. Configuring Anion-Exchange Membranes for High Conductivity and Alkaline Stability by Using Cationic Polymers with Tailored Side Chains. *Macromol. Chem. Phys.* **2016**, *217*, 1108.
(17) Pan, J.; Chen, C.; Li, Y.; Wang, L.; Tan, L.; Li, G.; Tang, X.; Xiao, L.; Lu, J.; Zhuang, L. Constructing ionic highway in alkaline polymer electrolytes. *Energy Environ. Sci.* **2014**, *7*, 354.
(18) Dang, H.-S.; Jannasch, P. Anion-exchange membranes with polycationic alkyl side chains attached via spacer units. *J. Mater. Chem. A* **2016**, *4*, 17138.
(19) Marino, M. G.; Kreuer, K. D. Alkaline Stability of Quaternary Ammonium Cations for Alkaline Fuel Cell Membranes and Ionic Liquids. *ChemSusChem* **2015**, *8*, 513.
(20) Mohanty, A. D.; Tignor, S. E.; Krause, J. A.; Choe, Y.-K.; Bae, C. Systematic Alkaline Stability Study of Polymer Backbones for Anion Exchange Membrane Applications. *Macromolecules* **2016**, *49*, 3361.
(21) Weiber, E. A.; Jannasch, P. Ion Distribution in Quaternary-Ammonium-Functionalized Aromatic Polymers: Effects on the Ionic Clustering and Conductivity of Anion-Exchange Membranes. *ChemSusChem* **2014**, *7*, 2621.
(22) Wang, C.; Shen, B.; Xu, C.; Zhao, X.; Li, J. Side-chain-type poly(arylene ether sulfone)s containing multiple quaternary ammonium groups as anion exchange membranes. *J. Membr. Sci.* **2015**, *492*, 281.
(23) Weiber, E. A.; Jannasch, P. Polysulfones with highly localized imidazolium groups for anion exchange membranes. *J. Membr. Sci.* **2015**, *481*, 164.
(24) Weiber, E. A.; Meis, D.; Jannasch, P. Anion conducting multiblock poly(arylene ether sulfone)s containing hydrophilic segments densely functionalized with quaternary ammonium groups. *Polym. Chem.* **2015**, *6*, 1986.
(25) Wang, C.; Xu, C.; Shen, B.; Zhao, X.; Li, J. Stable poly(arylene ether sulfone)s anion exchange membranes containing imidazolium cations on pendant phenyl rings. *Electrochim. Acta* **2016**, *190*, 1057.
(26) Weiber, E. A.; Jannasch, P. Anion-conducting polysulfone membranes containing hexa-imidazolium functionalized biphenyl units. *J. Membr. Sci.* **2016**, *520*, 425.
(27) Wu, W.; Wei, B.; Feng, J.; Chi, B.; Liao, S.; Li, X.; Yu, Y. Synthesis and Properties of Symmetric Side-Chain Quaternized Poly(Arylene Ether Sulfone)s for Anion Exchange Membrane Fuel Cells. *Macromol. Chem. Phys.* **2018**, *219*, 1700416.
(28) Lee, S.-W.; Chen, J.-C.; Wu, J.-A.; Chen, K.-H. Synthesis and Properties of Poly(ether sulfone)s with Clustered Sulfonic Groups for PEMFC Applications under Various Relative Humidity. *ACS Appl. Mater. Interfaces* **2017**, *9*, 9805.
(29) Chen, J.-C.; Liu, Y.-T.; Leu, C.-M.; Liao, H.-Y.; Lee, W.-C.; Lee, T.-M. Synthesis and properties of organosoluble polyimides derived from 2,2′-dibromo- and 2,2',6,6'-tetrabromo-4,4'-oxydianilines. *J. Appl. Polym. Sci.* **2010**, *117*, 1144.
(30) Chen, J.-C.; Wu, J.-A.; Chen, K.-H. Synthesis and characterization of novel imidazolium-functionalized polyimides for high temperature proton exchange membrane fuel cells. *RSC Adv.* **2016**, *6*, 33959.
(31) Chen, J.-C.; Chen, P.-Y.; Chen, H.-Y.; Chen, K.-H. Analysis and characterization of an atropisomeric ionomer containing quaternary ammonium groups. *Polymer* **2018**, *141*, 143.
(32) Nam, J.; Chippar, P.; Kim, W.; Ju, H. Numerical analysis of gas crossover effects in polymer electrolyte fuel cells (PEFCs). *Appl. Energy* **2010**, *87*, 3699.
(33) Baik, K. D.; Kong, I. M.; Hong, B. K.; Kim, S. H.; Kim, M. S. Local measurements of hydrogen crossover rate in polymer electrolyte membrane fuel cells. *Appl. Energy* **2013**, *101*, 560.
(34) Dekel, D. R. Review of cell performance in anion exchange membrane fuel cells. *J. Power Sources* **2018**, *375*, 158.
(35) Carmo, M.; Doubek, G.; Sekol, R. C.; Linardi, M.; Taylor, A. D. Development and electrochemical studies of membrane electrode assemblies for polymer electrolyte alkaline fuel cells using FAA membrane and ionomer. *J. Power Sources* **2013**, *230*, 169.
(36) Sung, S.; Mayadevi, T. S.; Chae, J. E.; Kim, H.-J.; Kim, T.-H. Effect of increasing hydrophilic-hydrophobic block length in quaternary ammonium-functionalized poly(ether sulfone) block copolymer for anion exchange membrane fuel cells. *J. Ind. Eng. Chem.* **2020**, *81*, 124.
(37) Lu, W.; Shao, Z.-G.; Zhang, G.; Zhao, Y.; Li, J.; Yi, B. Preparation and characterization of imidazolium-functionalized poly (ether sulfone) as anion exchange membrane and ionomer for fuel cell application. *Int. J. Hydrogen Energy* **2013**, *38*, 9285−9296.

(38) Guo, D.; Lai, A. N.; Lin, C. X.; Zhang, Q. G.; Zhu, A. M.; Liu, Q. L. Imidazolium-Functionalized Poly(arylene ether sulfone) Anion-Exchange Membranes Densely Grafted with Flexible Side Chains for Fuel Cells. *ACS Appl. Mater. Interfaces* **2016**, *8*, 25279−25288.
(39) Lee, K. H.; Cho, D. H.; Kim, Y. M.; Moon, S. J.; Seong, J. G.; Shin, D. W.; Sohn, J.-Y.; Kim, J. F.; Lee, Y. M. Highly conductive and durable poly(arylene ether sulfone) anion exchange membrane with end-group cross-linking. *Energy Environ. Sci.* **2017**, *10*, 275−285.
(40) Zhao, B.; He, G.; El Hamouti, I.; Gao, L.; Liu, Y.; Deng, R.; Yan, X. A novel strategy for constructing a highly conductive and swelling-resistant semi-flexible aromatic polymer based anion exchange membranes. *Int. J. Hydrogen Energy* **2017**, *42*, 10228−10237.
(41) Mayadevi, T. S.; Sung, S.; Chae, J. E.; Kim, H.-J.; Kim, T.-H. Quaternary ammonium-functionalized poly(ether sulfone ketone) anion exchange membranes: The effect of block ratios. *Int. J. Hydrogen Energy* **2019**, *44*, 18403−18414.
(42) Li, S.; Pang, J.; Chen, Z.; Liu, D.; Han, Y.; Wang, K.; Huang, S.; Jiang, Z. A high-performance anion exchange membrane based on poly(arylene ether sulfone) with a high concentration of quaternization units. *J. Membr. Sci.* **2019**, *589*, 117266.
(43) Ingabire, P. B.; Pan, X.; Haragirimana, A.; Li, N.; Hu, Z.; Chen, S. Enhanced conduction capability of nanocomposite membrane of quaternized poly (arylene ether sulfone)s covalently bonded with graphitic carbon nitride nanosheets for fuel cells. *React. Funct. Polym.* **2019**, *144*, 104260.
(44) Li, S.; Zhang, H.; Wang, K.; Yang, F.; Han, Y.; Sun, Y.; Pang, J.; Jiang, Z. Micro-block versus random quaternized poly(arylene ether sulfones) with highly dense quaternization units for anion exchange membranes. *Polym. Chem.* **2020**, *11*, 2399−2407.
(45) Koilpillai, S. S.; Dharmalingam, S. A novel quaternized poly(ether sulfone) membrane for alkaline fuel cell application. *Int. J. Energy Res.* **2015**, *39*, 317−325.

https://dx.doi.org/10.1021/acsaem.0c02734
ACS Appl. Energy Mater. 2021, 4, 2201−2217